EXTREME MAXIMUM AND MINIMUM TEMPERATURE TENDENCIES OVER TURKEY WITHIN LAST THREE DECADES

Yurdanur Ünal

Istanbul Technical University, Department of Meteorology, Maslak, Istanbul, Turkey
sunal@itu.edu.tr

ABSTRACT

Extremely low temperatures are expected to decrease continuously as global average temperatures rise. Extremely high temperatures are also expected to become more frequent and to occur for more extended periods of time with the continued global warming. Moreover, in some regions, it has been detected that there are significant increases and decreases in extreme temperatures over time.

A small change in mean temperatures is not necessarily related to small changes in the extreme values. A small increase in the mean temperature might have large changes in maximum or minimum temperatures due to the changes in the distribution function. Frich et al. (2001) found that number of days with frost is decreased on many regions of the globe and a statistically significant decrease in the difference between the annual extremes of daily maximum and minimum temperatures during the second half of the 20th century. On the other hand, Michaels et al. (2000) found that cold season in the mid- to high latitudes is warming up.

The purpose of this study is to determine tendencies of extreme maximum and minimum temperatures over Turkey. Therefore, maximum and minimum daily temperatures are analyzed for the period of 1975-2005, with the total of 31 years. Daily temperatures are recorded on 286 meteorological stations. Their distribution over Turkey is considerably uniform. Station data are carefully examined to identify nonhomogenous data sets. Data are subjected to Standard Normal Homogeneity Test, Buishand Rank Test, Von Neumann Ratio Test and Pettitt Test. Then, for each month, trend analysis is performed on extremes (5th percentile of minimum temperatures and 95th percentile of maximum temperatures).

Generally, positive trends of 95th percentile maximum temperatures are obtained in winter months over most parts of Turkey, reaching up to 1.2°C/decade in the central Anatolia while negative trends in 5th percentile of minimum temperatures are detected except for January. The results indicate that difference between extreme cold and warm temperatures increases during winter within last three decades. However, during the summer months, both trends are positive, and maximum temperature extremes are increasing on the western part of Turkey more than the eastern part of Turkey.

APPLICATION OF UNDERGROUND DAMS FOR GROUNDWATER AQUIFER RECHARGE AND CONTROL OF QANATS WATER

Mohammad Reza Yazdani[1], Korosh Shirani[2], Feizollah Rahnama [3] Morteza Khodagholi [4], Mohammad Azad[5]

1,2,4) Agriculture and Natural Resources Research Center, Isfahan, Iran,
moreya1@yahoo.com
3,5)watershed management, Natural Resources Department, Isfahan, Iran

ABSTRACT

The major center of existence Qanats are located in Iran, which have old history. To conservation of Qanat it is necessary to protection of groundwater and control of its exploration. Qantas drainage and flow to the lowland, when there is not use, therefore the water is wasting. This problem is intensify in winter season, especially. New technologies can have effective role in irrigation systems, but these require to comprehensive studies. One of the suitable approaches for groundwater recharge, yield improvement and control of Qanat water is use of underground dams, which can be applied in two ways: first is construction of underground dams in suitable place to cut of groundwater flow and water storage. Thus it can cause groundwater recharge and preventing wasting of water. Secondly, is use of underground dams, as like dike or wall in Qanat system to detention water occasionally and delay flow until the time of usage. In this study different conditions for damming in groundwater are evaluated for groundwater recharge and control of Qanat water.
Keywords: Qanat, Groundwater, Underground Dams.

INTRODUCTION

Qanats have been distributed throughout the world. Henry Beglo believes that Qanat was firstly invented in Northwest part of Iran to discharge groundwater in 800 B.C. Qanats were constructing in everywhere that water could be found. The number of Qanats in Iran sum up 18000 which Yield 7.5 billion cubic meters water per year. Although Qanat has been constructed for water utilization in agriculture, livestock and drinking water, it also followed has other objectives. It should be noted that Qanat and its relevant system had the most developed results in Iran, afterward has been extended to Mediterranean and South America region (Beaumaont, 1971)(figure 1).
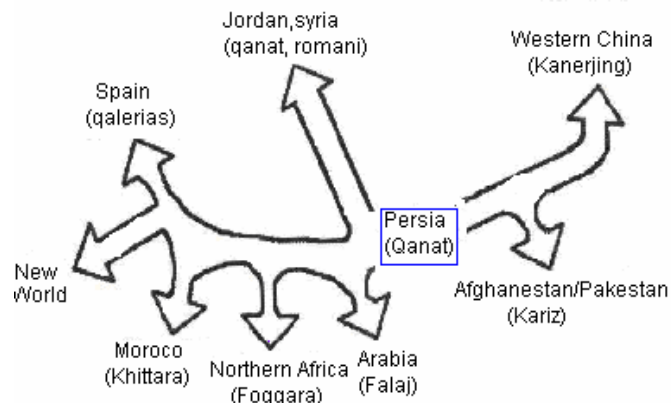
Figure 1. Qanat extension from Iran

Qanat is a system for using groundwater that it flows from upper lands aquifer. It is a technology from ancient era. It delivers groundwater to the farmland using gravity and save it from aridity during a year (Semsaryazdi, 2000). This Simple technology, don't need to vehicle and fuel and has low cost compared with well and its application in mountainous region are its advantages. It has mobility in use of a whole aquifer. However it may flows without control and can cause waste of water. It has limit application in smooth lands and vulnerable to natural disaster such as flood and earthquakes. No control of water discharge may be it's the most important disadvantage of a Qanat (Iranmanesh, 1982; Beaumoant, 1987; Dastorani, Saroghad, Reeisi, 2000). Qanat is permanent system of water discharge and the rate of discharge depends on different factors. Nowadays, Qanats has been dried up due to the modern technology such as wells. Destruction of Qanat is not only a water utilization system but also it is a culture. Regard to water shortage in the world; we need to reconstruct the Qanats. Development, improvement and proper utilization of water based on its natural condition is essential. Artificial recharge is referred to as a new method for Qanat development. Modern technology can help traditional systems such as Qanat, but it is require to through studies. Since a large part of Qanats water has discharged during non-cultivation period of a year, finding a method for reserving of water is inevitable. In figure 2 showes a general schematic of Qanat.
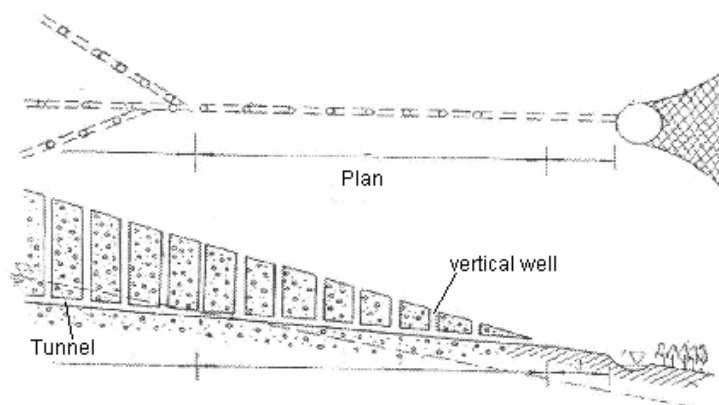

Figure2. General schematic of a Qanat

Control of Qanat discharge

Usually Qanats discharge in the winter is more than summer season, while the demand for water is increasing due to the cultivation practices in summer season. Permanent flowing of Qanats during the year, can causes high waste of water. This problem is a general defect of Qanats in Iran. Most often, water cannot infiltrate in ground and it flows as overland to the natural drainage systems, swamp, dry lands and salt lakes. This problem causes negative affect on an environment. To Utilization and reuse of water and water infiltration in the ground, need to energy and cost.

QANAT IMPROVEMENTS

There are several methods for flow control and retention of water in the ground layer. As an illustration, along the vertical airshafts, water can control using different structures such as a dike (Figure 3). This method is practical where the walls of a well are made of heavy clay during fall and winter season. This system depends on a few factors such as the length of Qanat, depth of the first well, volume of gallery and vertical airshafts and infiltration rate of water along dry wells. It is also possible creation a reservoir with watertight in the tunnel section (figure 4).

Control of flow dry wells: Infiltration rate along dry wells is very important. Since infiltration rate relates to square height of water, increasing of water pressure tends to cause rising in infiltration rate. Although, the length and volume of vacant space is high, infiltration has a disadvantage. In some cases, back-movement of water along dry wells tends to its falling out of upper land wells.
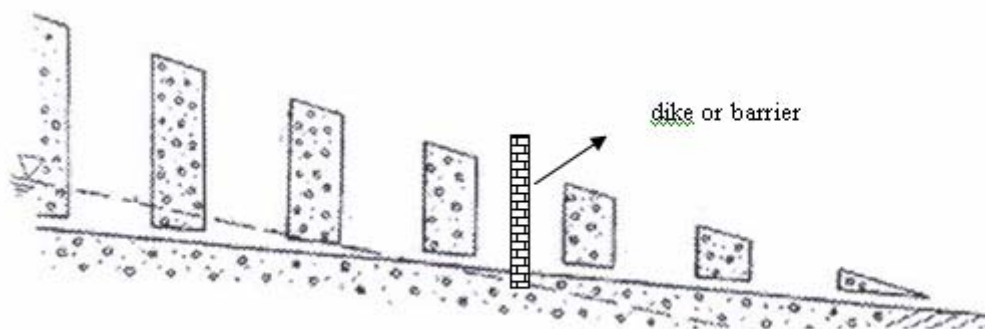

Figure 3. Dike creation in the well of Qanat

Control of flow along wet wells: The length of wet wells part is less than dry wells part. This part can cause water recharging. Control of flow can causes reduction of runoff. However it should be noted that soil saturation, can rising of groundwater table that it tends to decline of Qanats discharge.

Qanat lock: Some references refer to a three regulation gates which these can locked during the wet seasons when it is not requirement to water. These prevent of water loss. The locks are made of stone and each is located one meter apart from the other. They may made of stone and Sarooj. The locks have closed by a man who named Dashtban during winter

(Semsaryazdi, 2000).There are many traditional systems for Qanat improvements, that some of these made for flood control such as Shotorgelo(Papeliyazdi, 1992;Fakhartehrani, 2000).
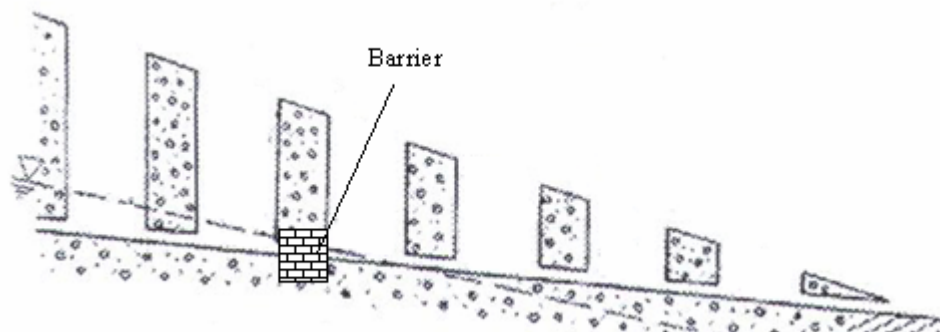

Figure 4. Barrier creation in the tunnel (Koreh) of Qanat

Underground dams: Numerous improvement systems have been innovated since beginning of Qanats' date. Ground-water dam is one of these methods for controlling Qanats flow. The Qanat of Vazvan is famous for its weirs that had constructed in front of its gallery (Figure 5). This weirs help to retention of water during winter for further usage in cultivation. This Qanat date back the emperor of Sasanian (Safinejad, 2000). It consists of 3 ground-water dam with gates that are opened based on the water level. This system is used from the end of fall to the preliminary of spring season. In this system a few gates in the same distance are constructed on a weir. These gates are closed during the non-cultivation period and gradually are opening in necessary time. The man who named Moghani with high experiences had design this kind of underground dams considering local conditions. This dike made up with especial material, that it named Sarooj. In these systems one vertical well (shaft) have been larger and then a dyke constructed in this section of Qanat (Behnia, 1988). Amin and et al (1998) studied several Qanats that have located in the Yazd province. They considered those, which are not subject to collapsed during rising of water table. After determining the boundary between wet and dry wells parts, they installed a tap on a weir based on the water discharge and flow had controlled during the year. Results indicate that efficiency of this method have 26 and 887 times extra cost compared with digging well or new Qanat, respectively. Also they noted that Qanats will remain longer than wells. He noted that about 25 percent of Qanats in Iran can be improved using this technique Engelish(1997) indicated that water utilization using wells without considering the appropriate discharge based on aquifer yield can causes land degradation, while Qanats' discharge are based on ground water table.
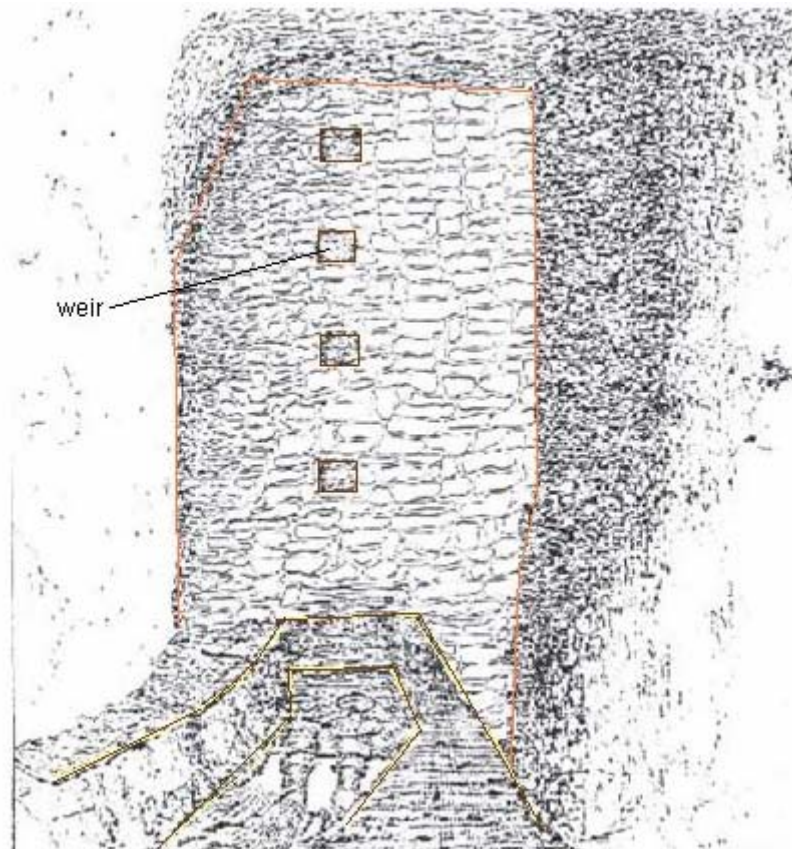
Figure 5. Underground dam in Vazvan Qanat

IMPROVEMENT OF QANATS DISCHARGE USING ARTIFICIAL RECHARGE

Artificial recharge is an appropriate method for increasing water discharge. Reduction of evaporation, temperature adjustment and pollutants treatment of water are accounted the advantages of artificial recharge. Generally, groundwater is preferred than other water resources due to its physical and chemical characteristics. This is basically true in the industrial regions where surface water is contaminated by wastewater of cities and factories. The main factors, which should be studied for artificial recharge, consist of geology, soil qualified and quantities properties of water (Attarzadeh, 1974). A few traditional methods for Qanats water utilization are following:

Goorab: In some parts of Yazd such as Dehbala and Meriz, small and big holes were diged and water can infiltrate. In winter, overland flow is delivered to these holes and water can infiltrate.

Houshab: in southeast part of Iran, Beluchestan, constructing small dams on the waterways can control floods. Its reservoir was filled with sediment that transported from farmlands. Groundwater recharge is the main objective of these dams.

Wadar: In mountainous region of Yazd, overland flow along the river networks was controlled using check dams (Janebollahi, 2000).

La:In many parts of Iran, especially where chains of Qanats can be found, two big channels were constructed in vertical airshafts it naming"La". These channels have two main objectives: Firstly, it can control of overland flow and prevention of its movement to the Qanats wells. Secondly, is retention of Qanat water located in upper lands in "La" system of lower land's Qanats, therefore period of overland flow is decreased. This system has a good efficiency, yet it faces with some problems such as evaporation. In some area where the system cannot be practiced, runoff can be deliver to the marginal lands around the villages for irrigating trees.

Groundwater dams: In previous section a type of groundwater dam was discussed which are constructed in the gallery of a Qanat. Another type of ground-water dam is constructed at upper land that it can causes rising of groundwater. Groundwater dam is constructed for different purposes such as prevention of salty water to the fresh water (Aoi, 1992), drought mitigation, prevention of surface water saltation, retention of water for dry season and improvement of Qanats discharge. These are the advantages of underground dams. Since Qantas water has less concentration of sediments and pollutants than surface water, it is preferred. These dams can be classified in to two groups including subsurface dams and sand dams. Subsurface is constructed in underground and reserves natural flow of aquifers, while the others reserve water on the sediment, which is deposited by a dam. Water-bearing formation consists of permeable alluvial deposition in a valley that it is for construction of wells. Aquifer is discharged during a year and causes dried wells out. To preventing this problem, a wall is constructed in the valley that gets in to though with bedrock. It causes the reservoir to be filled with water during the wet period. Excess water flows over the wall recharge the plain (Nillson, 1988; Tabatabaie, 2000). Figure 6 shows a typical groundwater dam.
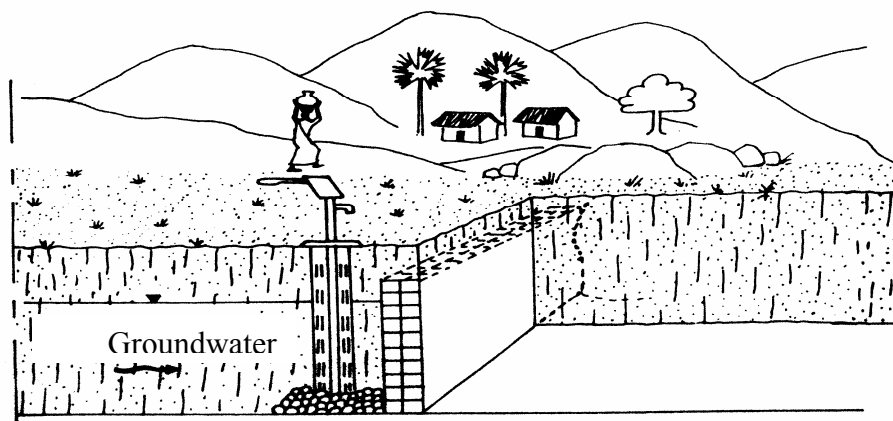

Figure 6. Groundwater dam for water use and groundwater recharge

RESULTS

Some places such as cities affect Qanats water, and can reducing its quality (Helweg, 2000). Technology of the well has a negative effect on groundwater resources. A total volume of 700 billions cubic meters have been utilized from groundwater resources in 2000.Deep and semi-deep wells and Qanats with 60 and 12 percent respectively are the most important methods of

groundwater utilizations (Haeri, 2003). Qanat is not only an engineering innovation but also is a social behavior, which affect its environment. Inappropriate systems and Cultivation pattern can cause Qanat dying. Droughts intensify this problem, so that more than 2500 Qanats of Yazd province has recently been dried up (UN mission report). Different reasons for drying Qanats have been reported. Wessels (2001) suggests that Qanat hasn't previous role for water supply because of daily-increasing demand of water. He believes that the only reason for Qanats drying is that human is being developed. In the past, agriculture had a close relationship with Qanats but appearance of new technology such as wells has affected this relationship. Regarding to the specific characteristics of arid and semi-arid regions, Qanat is still the best method of water utilization in these area. The importance of water resources in such area tends to apply existing resources but improvement or construction new Qanats need to pre-studies. Groundwater dam is an approach for prevention of runoff wasting as well as improvement of water resources in both aspects of quality and quantity. Regard to advantages of groundwater dam in improvement of Qanat system, it is necessary to integrated management in researches and executives programs, that it can provide us sustainable development.

REFERENCES

Ahmad, sh. And et al. (2004). Drought mitigation in Pakistan: current status and options for future strategies, international water management Institute, Drought series, paper 3.

Afkhami, A.A.(1997). Disease and water supply: the case of cholera in 19th century Iran, Middle Eastern Natural Environment, Bulletin 103, pp. 206-220.

Amin, S., Mirmohammadsadeghi, J. and Salimimonshadi, M.A.(2000). Water serving engineering in Qanat and its economical evaluation, Qanat articles collection, Yazd Regional Water Company, Yazd, pp.277-292.

Aoi, t. and et al.(1992). A Construction of subsurface dam at Nakajima II, IRCSA Regional Conference, PP. 644-684.

Atarzadeh, A.K.(1974).Artificial recharge of groundwater aquifer, Golshan publication., Tehran.

Beaumont, p.(1971) Qanat system in Iran, Bulletin of the International Association of Scientific Hydrology, 16(1), pp. 39-50.

Beaumont, p.(1987). The Qanat –a means of water provision groundwater source with reference to middle east, Proceeding of the Conference on Qanat systems in the middle East center of Near and middle Eastern, university of London.

8-Behnia, A. (1988).Qanat building and management, University publication center:Tehran.

Dostisani, M. (2000).Qanat effect on development of Mid-East region, Qanat articles collection, Regional Water of Yazd Company, Yazd, pp.25-38.

English, P.W.(1997). Qanats and life world in Iranian plateau villages, YALEF&ES Bulletin, PP. 187-205.

Fakhretehrani, F.(2000).Application of traditional materials in Iran Qanat, Qanat articles collection, Yazd Regional Water Company, Yazd, pp.187-204.

Haeri, M.R. (2003). "Kariz (Qanat): An Eternal friendly system for harvesting ground water, Adoption workshop, Newdelhi.

Helweg, O.J.(2000). Water for a growing population water supply and groundwater issues in developing countries, water international, VoL.25, PP. 33-39.

Iranmanesh, M.H. (1382).Qanat: rebuilding, improvement and yield increasing, Publication of Iran Geology organization.

Janebollahi, M.S.(2000).Traditional technologies for Qanat protection in desert regions, Qanat articles collection, Yazd Regional Water Company, Yazd, pp.205-234.

Kielstra, N.O. (1987). The transformation of a Qanat system Istahbanat, Proceeding of the Conference on Qanat systems in the middle East center of Near and Middle Eastern, University of London.

Nillson, A.K.(1988).Groundwater dams for water supply in small scale, International technology Publication, UK, 1988.

Papeliyazdi, M.H.(1992). Shotorgelo: suitable structure in semidry lands, geographical researches, seasonal series.

Reisiardakani, E.(2000).Hydrogeological conditions for Qanat protection or degradation, Qanat articles collection, Yazd Regional Water Company, Yazd, pp.235-244.

Safinejad, J and Dadres, B.(2000).Underground dam of Vazvan-Meimeh of Isfahan, Association of National westing of Iran Water Publication, Tehran.

Safinejad, J.(2000).Amusements of Iran Qanat, Qanat articles collection, Yazd Regional Water Company, Yazd, pp.59-80.

Saroghad, A. and Papeliyazdi, M.H. (1992). Qanat: a technology for water exploitation, ed: Hanri Gobloo, publication of cultural abroad of Astane Ghods Razavi.

Semsaryazdi, A. and Hadian, M.R.(2000).Study on plain Qanat degradation in Yazd province and protection approaches of it, Qanat articles collection, Yazd Regional Water Company, Yazd, pp.391-406.

Tabatabaieyazdi, J. (2000). Groundwater dam: a method for drought mitigation, First National conference on approaches for low water preparing and drought mitigation", Zabol.

UN Mission Report.(2000). United Nations technical mission on the drought situation in the Islamic Republic of Iran.

Wessels, J. and Hoogereen, R.J.A.(2002). Renovation of Qanats in Syria, ICARDA Projects.

THE CHANGES IN THE SUMMER SEASON LENGTH IN THE MIDDLE EAST

Yair Goldreich and Zipora Chermoni

Dept. of Geography and Environment, Bar-Ilan University,
Ramat-Gan, 52900, Israel goldrey@mail.biu.ac.il

ABSTRACT

The summer season in the Middle East is well defined synoptically and weather-wise, especially in the Mediterranean climate region. The Persian Trough dominates from June to September, accompanied by the Mediterranean High (a branch of the Azure Anticyclone) aloft. Rainfall amounts in June-August in Israel are nil, and weather fluctuations are minute. The stable air is caused by the thick upper inversion (basis below 1000 m ASL) which persists during 80% of the summer days. Due to the clear and unique definition of the summer season, it is relatively easy to define its period and to assess the inter-annual changes in its length. We examined ten weather and synoptical parameters and selected two parameters: The elevation of the tropopause (above 16,000 gpm for at least 10 consecutive days) at Bet-Dagan, Israel and the commencement and termination of the Persian Trough situation on the synoptic charts. These commencement and termination dates for both parameters, the length of the summer season as well as a combination of both, were collected over 25 years (1980-2004) and were subject to regression analysis and two trend tests (Mann-Kendall and Spearman rank statistics). The results reveal a very high significant trend in all the nine data sets, where the summer starts earlier and terminates later and the number of summer days increases over the years.

INTRODUCTION

Studying the inter-annual change in the seasonal length is not a simple task. The shift between seasons is not a clear cut event or date, but rather a prolonged unsmoothed transition of selected meteorological parameters or synoptic situations [1]. Even defining the beginning and termination of the mean season date is not obvious. In some countries the four seasons are almost equal-length using the arbitrary astronomical dates (solstices and equinoxes), which do not necessarily have a clear climatological meaning [4, 6].

However, in the Middle East the summer's synoptic situation is very a clear cut. The Persian trough dominates the whole summer, a phenomenon which allows us to determine the summer's commencement and termination easily. Consequently, we will utilize this phenomenon to determine changes in the length of the summer season together with another weather parameter. In the next section we shall present the summer situation, which will be followed by selecting the meteorological parameters which will serve as proxies for the summer commencement and termination. In the following section we shall explain the methods and finally we shall present the results of the trend test and some conclusions.

SUMMER CLIMATE IN THE MIDDLE EAST

Instead of the winter Siberian anticyclone, which dominates Asia during winter, in the summer there is a monsoon depression with its center over Pakistan, which has a persisting

trough towards the Middle East. This steady summertime barometric trough (the *Persian trough* or the *seasonal trough*) extends from the Persian Gulf through Iraq to Turkey and the northeastern Mediterranean Sea (Figure 1).
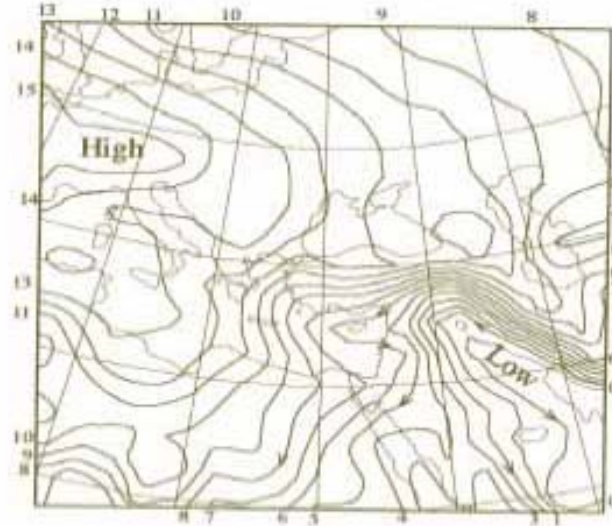

Figure 1 Mean June-September 1000 hPa height contours (1983-88). The interval is 10 m (geopotential), arrows show wind direction [after 1].

Due to this persisting synoptic condition, northwesterly winds prevail over the mountain region, in the Levant both day and night, for weeks and months, causing abundant dew towards the end of the summer. This is the marine *etesian flow* well recognized, by the ancient Greeks, as a typical eastern Mediterranean wind. The hot and dry desert flow, mainly from the east, (e.g. the sharavs in Israel), occur only during transitional seasons. Rare summer sharav conditions are a sign of an abnormal monsoon depression development.

Another connection between the Indian monsoon and the Levant summer weather may be discerned in the tropopause [5]. As in summer everywhere, the tropopause rises, but the wind speed in this layer is weakened due to the northward migration of the jet stream. This rise is expressed by the vanishing of the lower tropopause (9-12 km) and the appearance of the higher tropopause at 15-17 km. During the first week after the establishment of the summer monsoon in central India (end of May and the beginning of June), the radiosonde data at Bet Dagan (Israel) show an abrupt tropopause rise, connected with a southerly warm flow intrusion. This change indicates that our region commences its summer climate regime. In most of the Mediterranean climate regions in the Middle East the summer is rainless, where in the Levant coast the mean precipitation for June-August is nil. The lack of rainfall condition is due to upper inversion which prevails mainly during the summer season. This air stability explains the "summer paradox" [3], namely the lack of rain in an area of a barometric trough, on shore Etesian winds, high temperature and high humidity. This condition prevails the whole summer with monotonous weather, slight temperature and humidity fluctuations (the summer temperature daily standard deviation in Israel is between 0.5-1°C).

The synoptic situation transition from spring condition to the summer can be described in the following manner. In the spring, at the peak of the Red Sea trough, the Persian trough evolves

as another branch extending from the direction of the Arabian Sea. During May, both troughs compete for the dominance over the Middle East airspace. This trough migrates eastward over the Arabian Peninsula (named by the Israeli forecasters PARED [Persian-Red Sea]) and finally becomes part of the Southeast Asia monsoon over the Persian Gulf. While the spring-summer synoptic transition is gradual, the end of the summer condition is different. The termination of the Persian trough sometime in September, is quite abrupt, without a migration towards the Red Sea trough location.

DATA

Defining the summer season merely by the synoptic Persian trough has an obvious drawback. Sometimes it is somewhat subjective to determine if the trough is Persian or still a PARED. Therefore, we examine 11 meteorological parameters to define the summer season. They include upper inversion frequency and height, tropopause elevation in the eastern Mediterranean, wind shear and speed at this level, location and speed of the jet stream, mean temperature, mean relative humidity, Etesian wind direction, land and sea breezes, solar radiation intensity, fog frequency and cloudiness cover. Eventually it was found that the tropopause elevation parameter is the most suitable. The criteria of this parameter are the following: The first summer day is defined when in at least 10 consecutive days the tropopause base was above 16,000 gpm or lower than 110 hpa. The same criteria were applied for the summer termination: the last day of the last 10 consecutive days with these parameter combinations.

Data were obtained from the Israeli Meteorological Service radiosonde data and synoptic charts for a period of 25 years (1980-2004). Earlier data are not complete or were transfered to microfiches which lost their quality over the years. This study started some years ago when the new NCEP/NCAR daily reanalysis data were not available.

METHODS

Beside the separate dates determined by the synoptic situation and the tropopause location a third date was established – the combined date. The determination of the combined date for commencement and termination of the summer season was defined as the mean date between the synoptic and the tropopause parameter dates. In case of an even number of day gaps between the dates, the later date of the two mid-days was chosen. The summer length parameter was obtained by subtraction of the beginning date from the termination date. Altogether nine temporal data sets were analyzed.

Three trend tests were applied on each of the nine series: 1. Standard error of the regression coefficient. 2. Mann-Kendall trend against randomness. 3. Spearman rank statistics. The two non-parametric tests Mann-Kendall and Spearman rank were recommended by the WMO [7].

RESULTS AND CONCLUSIONS

Table 1 presents the results of the three tests. The first two columns contain the coefficients of the regressions and their standard errors. The next two columns represent the Mann-Kendall parameters P and τ. The following two columns display the Spearman Rank statistics

parameters. The last column shows the probability trend of the regression coefficients. All the probabilities of Man-Kendall and Spearman tests are <0.001, while in the last column which displays the probability of the regression coefficient there are some higher probability values. Figures 2-10 display the coefficient of determination (r^2), regression line and equation for each of the nine temporal data sets.

Table 1. Results of the trend tests and their significance [2].

Parameters	b	±SE$_b$	P	τ	r$_s$	t	.*Prob
Beginning of PT	-0.77	0.178	50	-0.67	-0.85	-7.79	<0.001
Termination of PT	0.59	0.139	259	0.73	0.90	10.1	<0.001
ST Beginning of	1.36	0.301	50	-0.67	-0.65	-4.1	<0.001
Termination of ST	-0.86	0.202	236.5	0.57	0.73	5.10	<0.005
No. of PT days	0.34	0.101	260.5	0.73	0.92	10.97	<0.001
No. of ST days	1.20	0.282	249	0.66	0.85	7.75	<0.001
Combined - Beginning	-081	0.105	52	0.65	-0.84	-7.57	<0.001
Combined - termination	0.43	0.188	263.5	-0.75	0.89	9.70	<0.02
No. of Combined days	1.28	0.285	264	0.76	0.92	10.9	<0.001

*All the probabilities for Man-Kendall and Spearman tests are <0.001
PT – Persian Trough
ST - Summer Tropopause
b – Regression coefficient
SE$_b$ – Standard Error of the Regression coefficient
In all parameters (for 95% probability): $(\tau)_t = \pm 0.27941$

According to the Persian trough, after 1988 in all the years the number of summer days were >70 and after 1996 >80 days. The mean date through the whole period is July 26th with a deviation of up to two days, except for 1981 where the mean date was July 31st and in 1989, July 22nd. The meaning of this mid-season date is that the summer season is getting longer in both directions. The variability of the tropopause parameter is higher than the synoptic one. Up to 1988 the summer tropopause condition did not pass the 72 days threshold and the mean until this year was 66 days. During 1990-9 the mean summer tropopause condition escalated to 83 days and in the past two years it passed the 90 days threshold. Comparison of the beginning and termination of the tropopause parameter is almost identical to that of the synoptic parameter date or appeared in a lag of some days but never preceded.

Figure 2. Coefficient of determination Linear Regression line and equation for the beginning date of the Persian trough

443
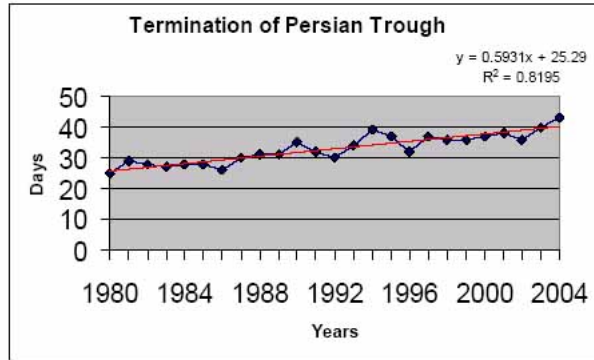
Figure 3. Coefficient of determination Linear Regression line and equation for the termination date of the Persian trough
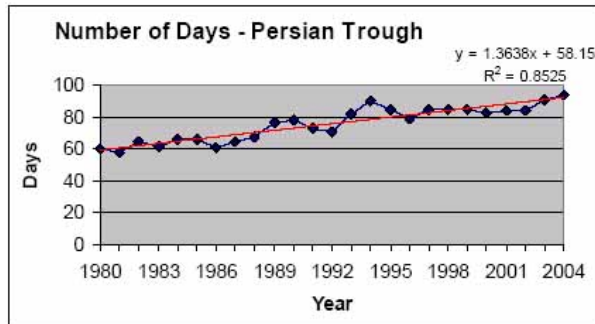

Figure 4. Coefficient of determination Linear Regression line and equation for the number of days of the Persian trough
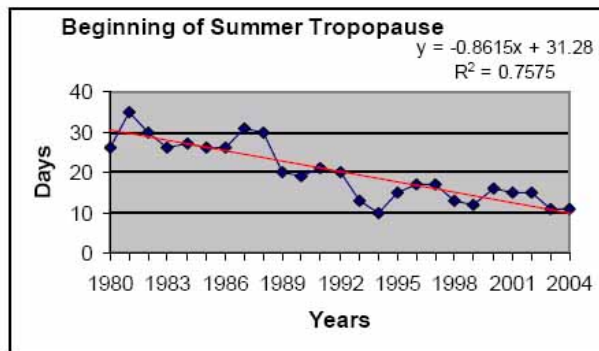

Figure 5. Coefficient of determination Linear Regression line and equation for the beginning of the summer tropopause
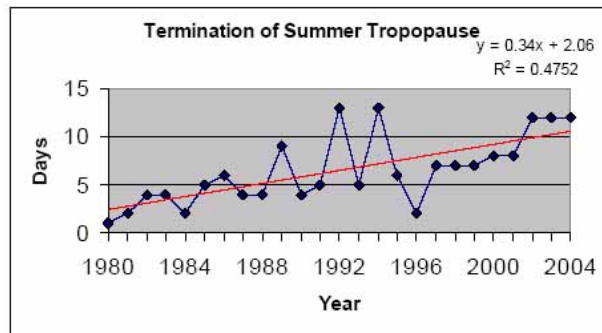
Figure 6. Coefficient of determination Linear Regression line and equation for the termination of the summer tropopause
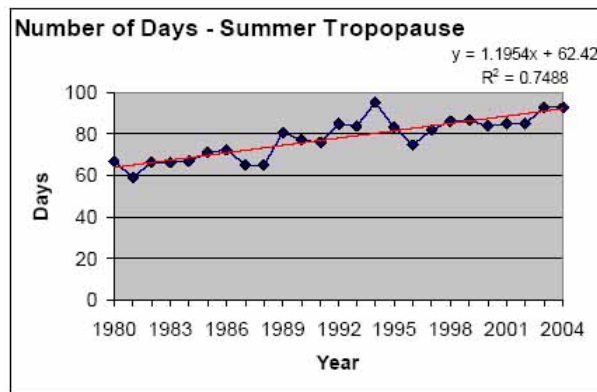

F**igure 7.** Coefficient of determination Linear Regression line and equation for the number of days of the summer tropopause
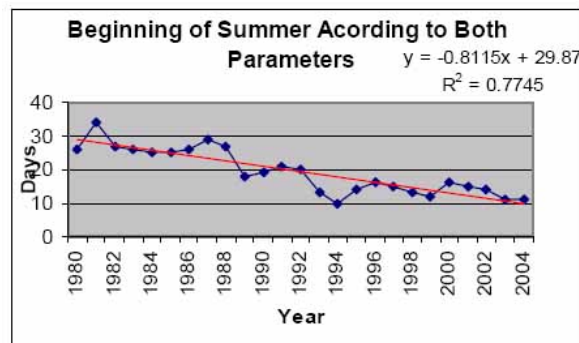

Figure 8. Coefficient of determination Linear Regression line and equation for the beginning of summer according to both parameters
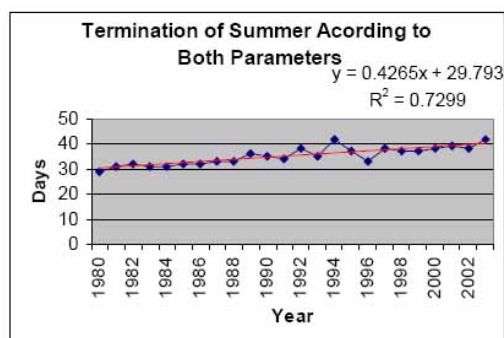
Figure 9. Coefficient of determination Linear Regression line and equation for the termination of summer according to both parameters
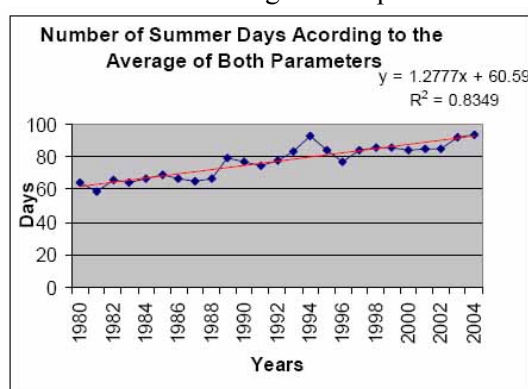

Figure 10. Coefficient of determination Linear Regression line and equation for the number of summer days according to the average of both parameters

We may conclude that the summer in the Middle East is getting longer; the beginning occurs earlier and terminates later. This trend is clearer than the little increase in the summer temperature (at least in Israel). It seems that the summer increase is on account of both transitional seasons. As for the cause of this trend, as yet there is no other explanation except than global warming.

REFERENCES

1. Alpert, P.*,* I. Osetinsky, B. Ziv & H. Shafir 2004: Semi-objective classification for daily synoptic systems: application to the eastern Mediterranean climate change. *Int. J. Climatol*, **24**, 1001-1011.

2. Chermoni, Z., 2005: The temporal variability of the summer season length in Israel, Master thesis, Department of Geography and Environment, Bar-Ilan University, Ramat-Gan, Israel (in Hebrew with English an extended English abstract)

3. Goldreich, Y. 2003: The Climate of Israel, Observation Research and Application. Kluwer Academic / Plenum Publishers, NewYork.

4. Ovadiah E, & Y. Goldreich, 1997: Year division in Israel according to temperature data. *Judea Samaria Res. Stud*., **6**, 293-297 (*in Hebrew*).

5. Shaia, J.S., 1974: The tropopause over the Eastern Mediterranean..*Isr.Meteorol. Service*, Series A, No. 31.

6. Trenberth, K. E. 1983. What are the seasons? *Bull. Amer. Meteorol. Soc.* **64**, 1276-1282.

7. W.M.O., 1966: Climatic Change, No. 195, TN 100, Geneva.

VARIATION OF GROWING SEASON LENGTH (GSL) OVER SECOND HALF OF 20TH IN IRAN

A. Sedaghat Kerdar and F. Rahimzadeh

Atmospheric Science and Meteorological Research Center (ASMERC),
P.O.Box 14965-114, Tehran, Iran, aseda@irimet.net

ABSTRACT

The variation of growing season length during the last decades is one of the important impacts of global warming. It has been intensified by occurrence of early spring and late autumn freezing. The length of growing season has been increased in mid and higher latitudes of the Northern Hemisphere in association with the global warming. For this purpose, there are varieties of indices, but it is necessary to introduce a plant-free definition for applications, such as climate models and it's changes for interpretation of global warming, appropriate description of forest and farm land. One of the definition is Growing Season Length (GSL) indices was defined by Commission for Climatology\ Climate Variability(CLIVAR). It is found by counting the number of days between first span of at least 6 days with daily mean temperature greater than 5° after July 1rst (Jan 1rst in Southern Hemisphere) and first span of 6 days with daily mean temperature less than 5°.

High quality and homogenous daily temperature data sets from 27 Iranian synoptic stations for period of 1951-2003 were used for the study of variation of GSL accompanied by number of Frost days and Icing days. It was found that these indices are not appropriate for stations like Bushehr and Abadan where located in southern part of the country. It was determined that there are positive trends for GSL in most of the stations where located in the central and northern parts of the country. The highest values of these trends, 7 to 12 days per decades belongs to Kermanshah, Mashhad and Tehran respectively. The number of Frost days has decreased in most of the stations too.

Keywords: global warming, climate change, indices, growing season length, homogeneity

INTRODUCTION

Global mean temperature have continued to raise over the last decades. Changes in cold extremes indices such as number of Frost days and Icying day's indices have been consistent with this warming [2; 3 and 4]. In contrast, increasing of climatological growing season length (GSL) have revealed during the last few decades due to increasing mean temperature over the most part of the world [5 and 6]. Globally, Frich et al [4] showed, a lengthening of the thermal growing season has been observed throughout major parts of the Northern Hemisphere mid-latitudes with the notable exception of Iceland.

The objective of this paper is to provide the analysis of GSL in association with FD and ID over the country. We used high quality data from 27 Iranian Synoptic stations. We determinated the linear trends of three indices including FD, ID and also GSL by Least Square Methods and Mann-Kendall test for testing the significant trends [8].

DEFINTIONS AND METHODS

For many purpose, description of forest and agricultural site, a general definition and plant independent is of interest. One of the definition is Growing Season Length (GSL) indices was defined by Commission for Climatology\ Climate Variability(CLIVAR). According to this definition GSL is defined by counting between first span of at least 6 days with

Daily mean temperature >5 º

after July 1rst (Jan 1rst in Southern Hemisphere) and first span of 6 days with

Daily mean temperature < 5°.

[9].

Other proxy indices to confirm increasing of minimum and maximum temperature and also the climatological growing season are Number of frost days(FD) and Number of Icing days(ID) that have reduced across the world. FD and ID are defined by counting of days when Daily minimum temperature < 0º and counting of days when Daily maximum temperature < 0º , respectively.

Due to the inhomogeneties problem such as relocation, exposure and instrumentation that affect mean climate values and also the extreme values of temperature, we selected the daily data of 27 Iranian synoptic stations, to produce the annual series of Number of FD, , ID and GSL.

We used least square methods for finding the linear trend. The nonparametric Mann-Kendall test was chosen for testing the significant trends, as it can be used with knowing the exact distribution of the time series [8].

RESULTS

The annual time series of FD, ID and also GSL for the period 1951-2003 for 4 selected station including Tehran-Mehrabad, Tabriz, Mashhad and Shiraz are displayed in Fig 1-4. Linear trends of 27 stations are showed in Fig 5 -7. Each map shows, whether the trend of series of station has been statistically significant or not. The most important results about these indices are as follow :

Number of Frost days and Icing days
Generally, trends in the number of frost days and icing days through most of the country with several significant negative trends found, mainly across Alborz mountain in northern parts and central of the country. However some station records (Oroomieh, Sharekord and Birjand) showed increasing trends for number of frost days . This result consistent with many previous studies which indicate the minimum temperature have increased over the country [7] but decreasing in these stations [1].

Of course , due to different climate in Iran, Stations located in south of Iran mostly have not experienced frost days and icing days such as Bandarabbas, hence description of trends of these indices can not be meaningful. It is not experienced icing days across Caspian sea stations too.

Growing season Length

The GSL index mostly showed a significant positive and positive trend during the period 1951-2003. The GSL for Mashhad, Kermanshah, Esphahan, Shiraz and Tehran-Mehrabad. station have increased about 20 days during the 1951-2003.

This definition were not able to be efficient for stations across Caspian sea, Persian Gulf and Oman sea. Generally, this index are generally not appropriate for the relatively warm climate The station located across Pesian Gulf and Oman sea such as Boushehr and Abadan in South of Iran.and also across Caspian Sea such as Bandar Anzali, Babolsar and Rasht stations have experienced more than 360 days each year during the 1951-2003.

 REFERENCES

1. ASMERC, 2005, National Project report on " reduction of chilling damage on agricultural products in provinces of east and west Azerbaijan (In Farsi)
2. Collins, D.A., P.M. Della-Marta,., N. Plummer, B.C. Ttrwin,. 2000: Trends in the frequencies of extreme temperature events in Australia. Australian Meteorological Magazine, 49, 277-292.
3. Easterling, D.R., J.L. Evans, P.Ya. Groisman, T.R. Karl, K.E. Kunkel, and P. Ambenje, 2000: Observed variability and trends in extreme climate events: A brief review. Bulletin of the American Meteorological Society, 81(3), 417-425.
4. Frich, P.L. and L. Alexander, P. M. Della-Marta, B. Gleason, M. Haylock, A. Klein Tank, T. Peterson. 2002: Observed coherent changes the second half of the twentieth century. Clim and Research, 19: 193-212.
5. Menzel A. 2003: Plant phonological anomalies in Germany and their relation to air temperature and NAO. Climate Change 57: 243-263.
6. Robeson SM. 2002. Increasing growing-season length in Illinois during the 20th century. Climate Change 52: 219-238.
7. Rahimzadeh, F., and Asgari. A, 2003: A Survey on Recent climate change over IRAN. Proceeding of 14th Global Warming international conference & expo (27-30 May, Boston, USA).
8.   Sneyers, R., 1990. On the Statistical Analysis of Series of Observations, WMO Publ. No. 415, Geneva.
9. URL1 – http:/ccma/seos.unic.ca/ETCCDMI
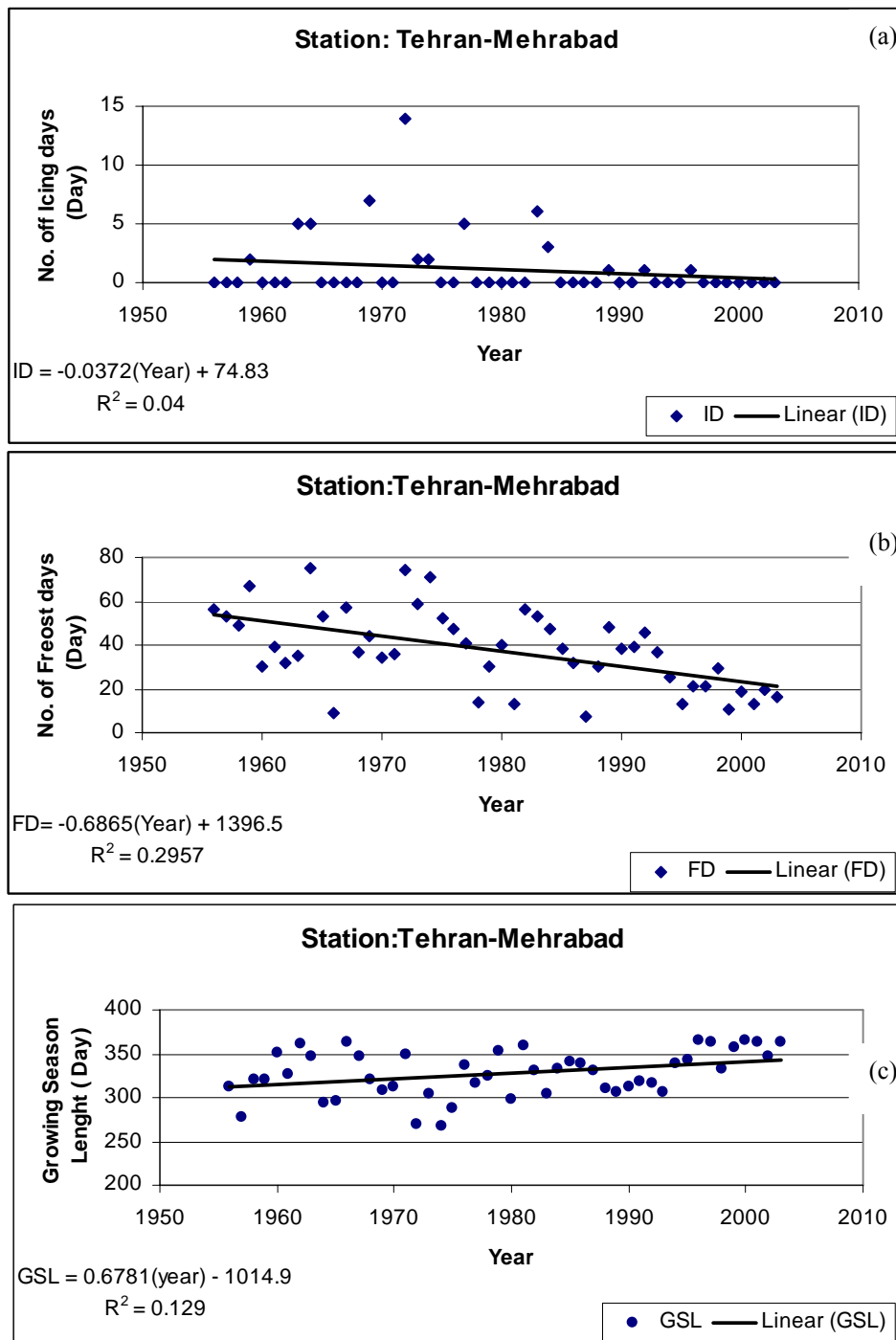
Figure 1. Linear trend of a) Number of Frost Days b) Icing Days and c) Growing Season Length(GSL) in Tehran-Mehrabad Station (1951-2003).
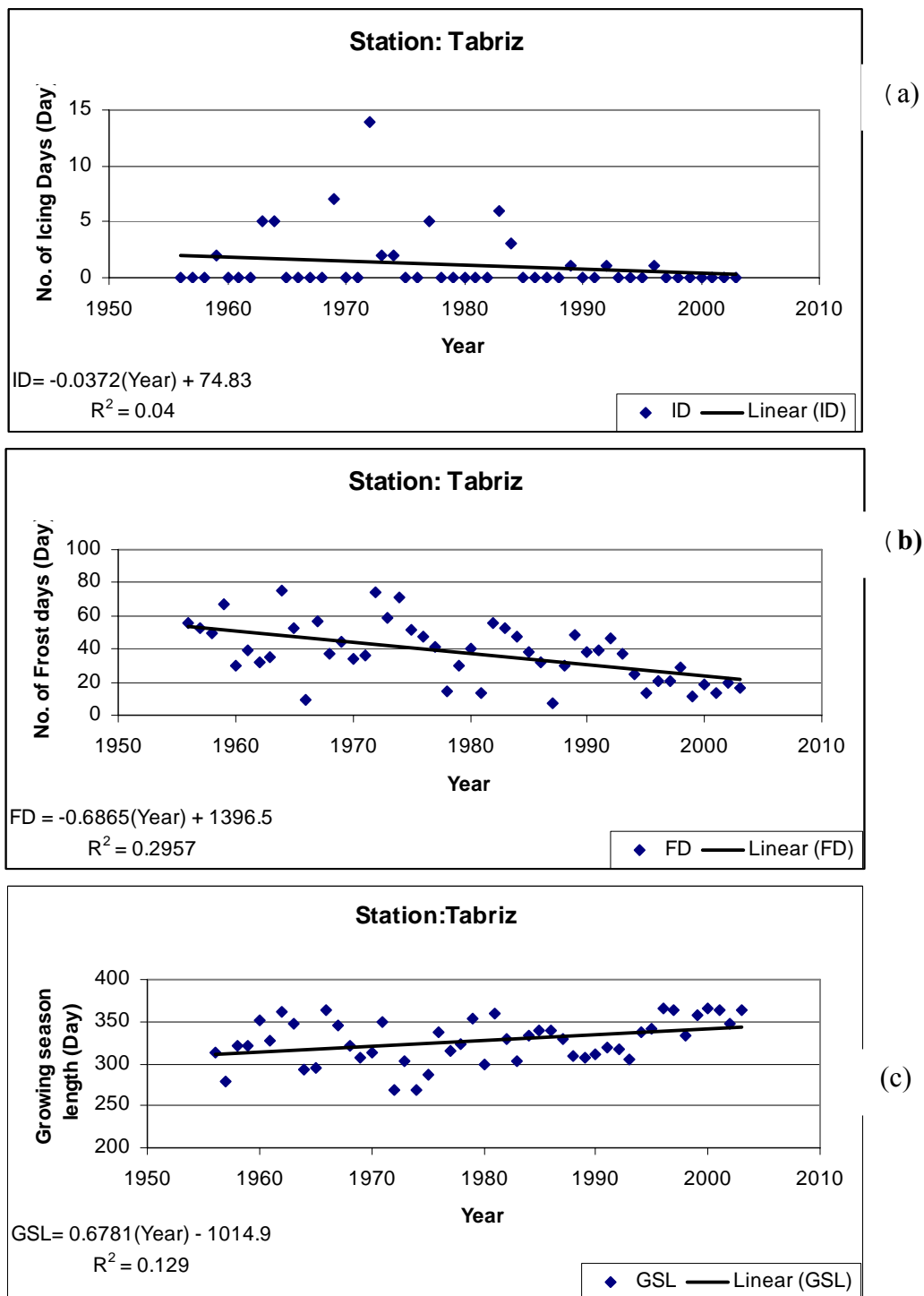
Figure 2. Linear trend of a) Number of Frost Days b) Icing Days and c) Growing Season Length(GSL) in Tabriz Station (1951-2003).
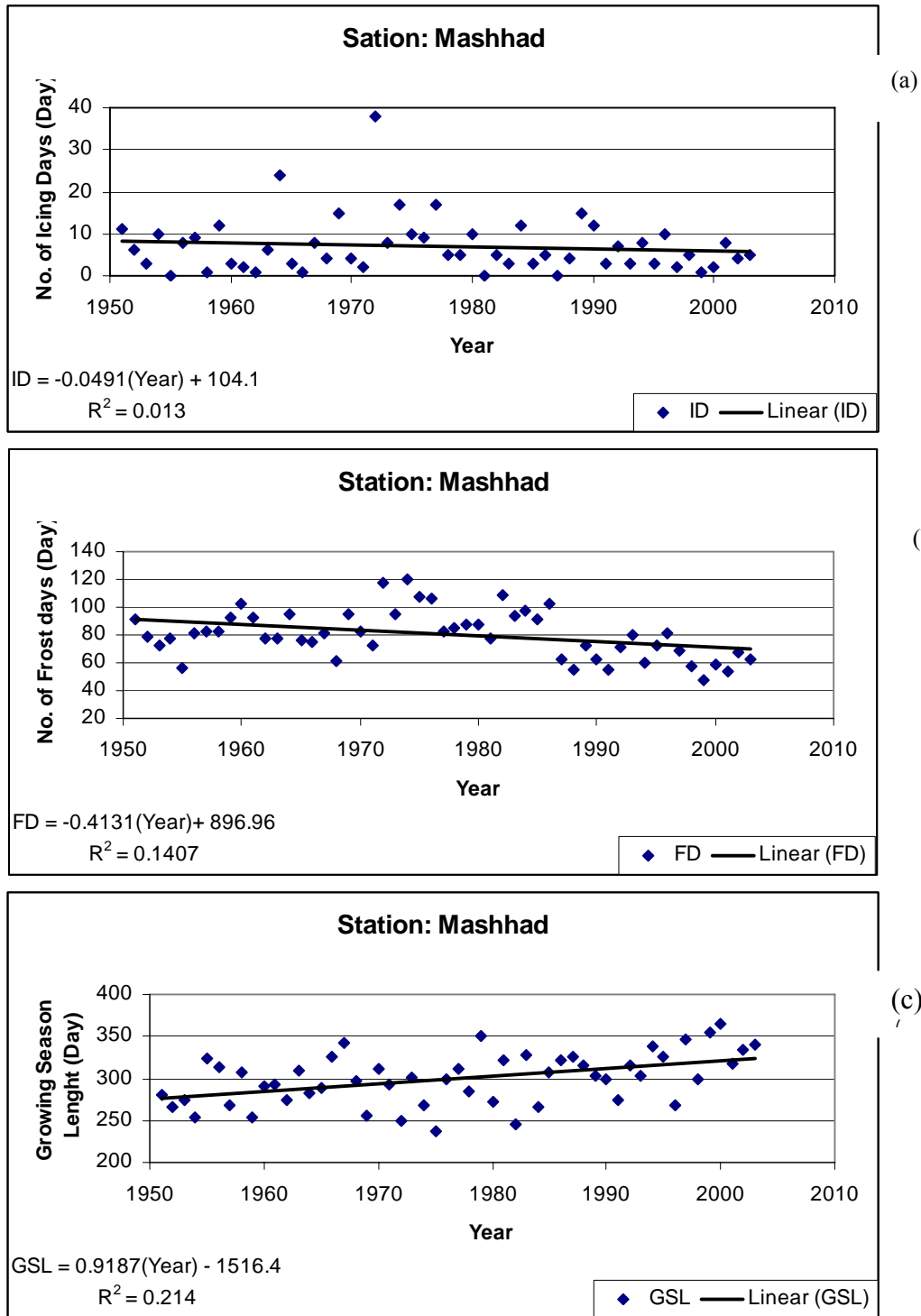
Figure 3. Linear trend of a) Number of Frost Days b) Icing Days and c) Growing Season Length(GSL) in Mashhad Station (1951-2003).
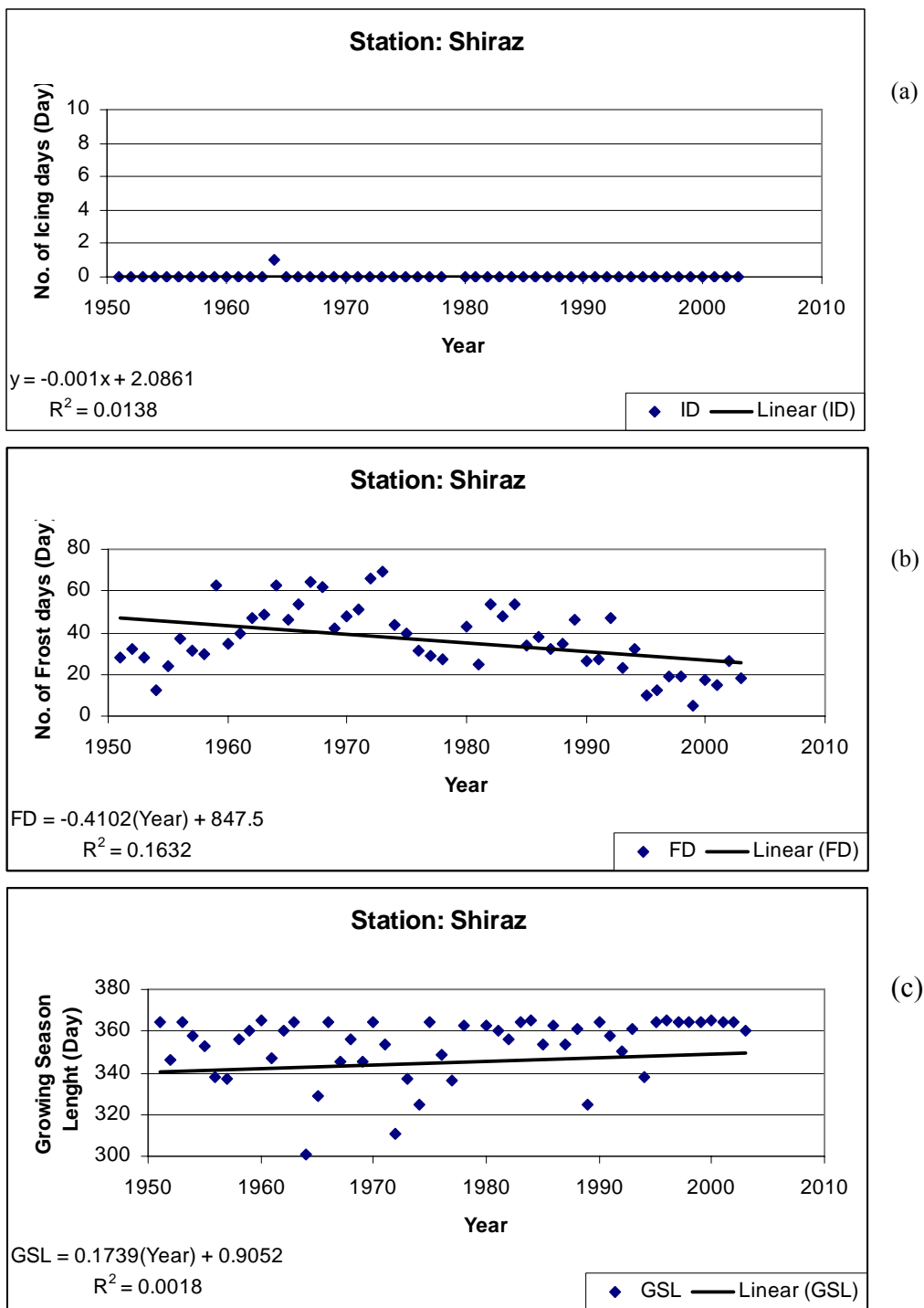
Figure 4. Linear trend of a) Number of Frost Days b) Icing Days and c) Growing Season Length(GSL) in Shiraz Station (1951-2003).
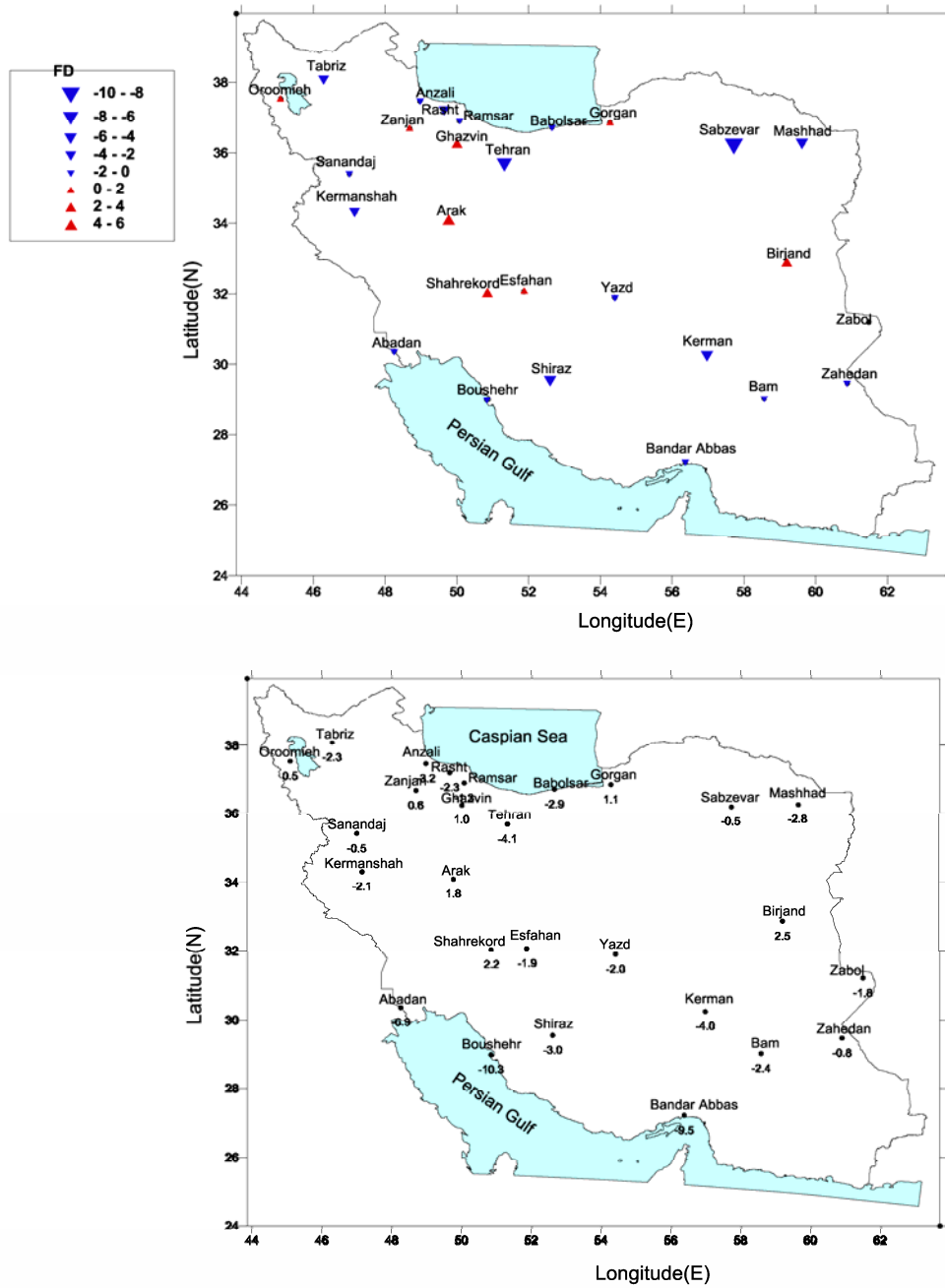
Figure 5. Decadal trends for Number of Frost Days (FD) index in selected Iranian synoptic stations for period 1951-2003.
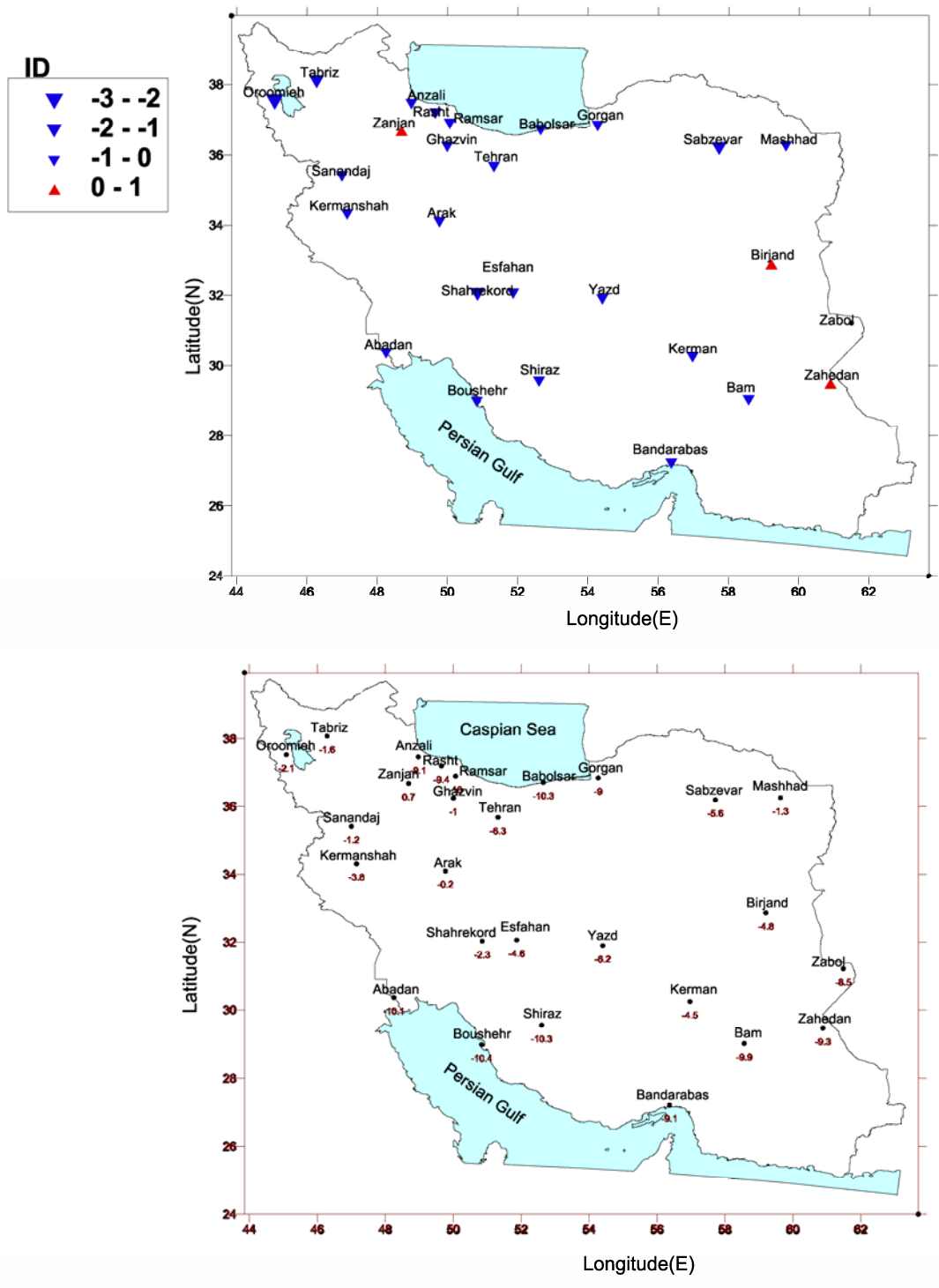
Figure 6. Decadal trends for Icing days(ID) index in selected Iranian synoptic stations for period 1951-2003.

455
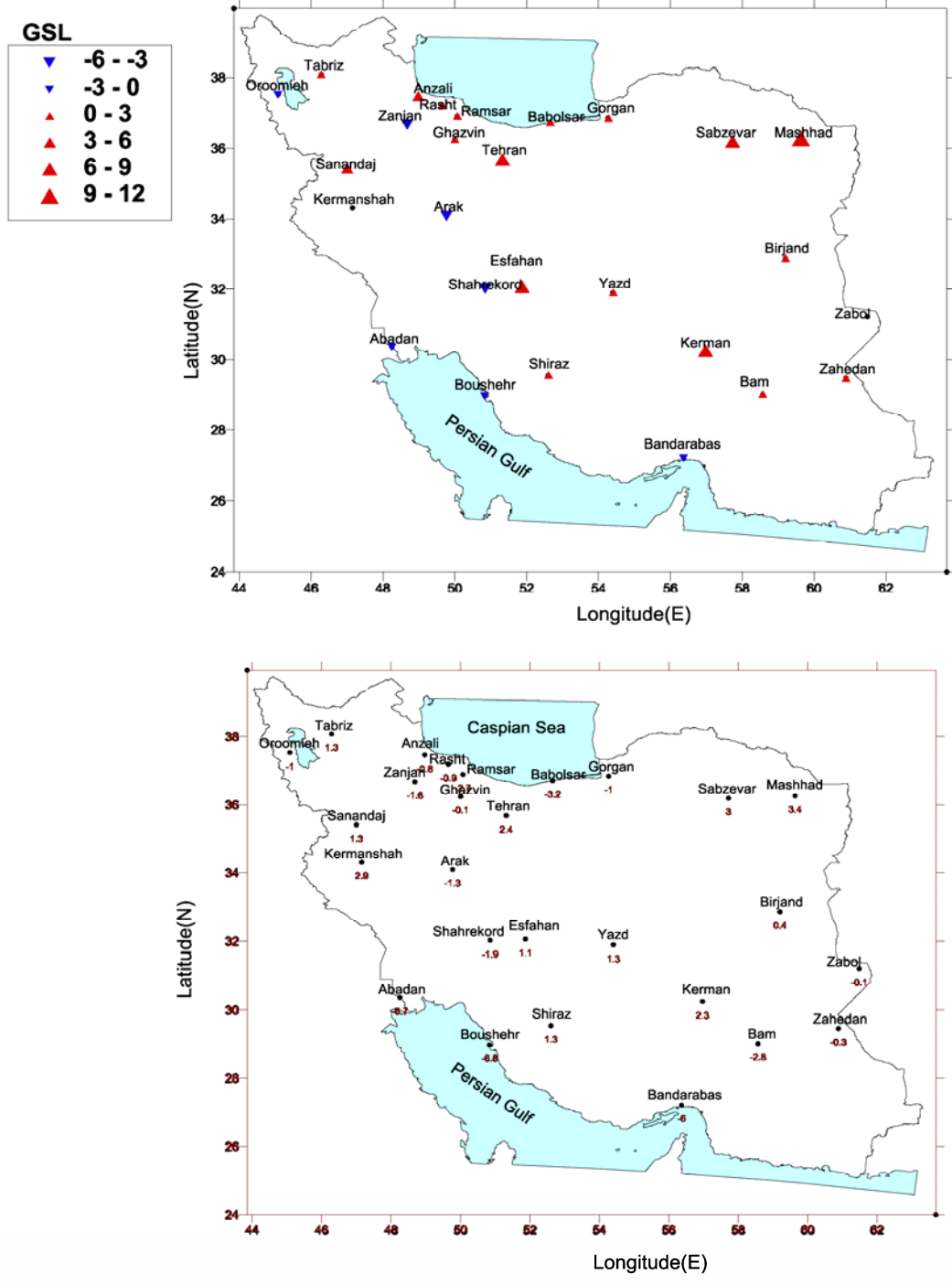
Figure 7. Decadal trends for Growing Season Length (GSL) index in selected Iranian synoptic stations for period 1951-2003.

THE CAMI PROJECT: NON-CONVENTIONAL SEISMIC ANALYSIS TO CHARACTERIZE THE SHALLOW AQUIFER

Umberta Tinivella, Flavio Accaino, Michela Giustiniani and Stefano Picotti

Istituto Nazionale di Oceanografia e di Geofisica Sperimentale – OGS, Borgo Grotta Gigante 42C, 34010, Trieste, Italy, utinivella@ogs.trieste.it

ABSTRACT
In the frame of the European project CAMI, several geophysical data were acquired to characterise the main aquifer (located) in the Friuli plain (North-East of Italy). The seismic data were processed with conventional and non-conventional analysis to better characterise the petro-physical properties of the subsoil. The detailed velocity model reveals the presence of lateral velocity variations and high velocities that could be associated to the saturated layers. The amplitude versus offset analysis recognises two main areas characterised by different seismic properties; anomalies of the main trends are associated to the fluid presence.

INTRODUCTION

We present the results of the non-conventional seismic analyses performed in the project entitled "Water-bearing characterization with integrated methods (CAMI)", supported by European community (LIFE; see details of the project in [1]). The site test is located in an area defined by the Tagliamento river (North-East of Italy; location map in [1]). During the last winter, we acquired three 2D seismic lines with the main purpose to determine a preliminary subsurface geometry and the seismic response to plan the 4D survey. In general, the quality of the data was satisfactory, even if the ground roll was strongly evident. The 2D stacked sections show the presence of reflections with lateral amplitude variations [1]. Thus, we performed a detailed velocity and amplitude versus offset (AVO) analyses to characterize the shallow structures; in this paper we present the main results obtained from the processing of the Line 2. The velocity field was obtained inverting the travel time table of the pre-stack data by using the commercial software CAT3D. The AVO analysis performed by using commercial software GeoDepth$^{©}$ (Paradigm Geophysical) has allowing obtaining petro-physical information about the main targets. The inputs were the seismic data processed with a true amplitude procedure and the detailed velocity field in order to translate the offset into incidence angle. The processing was focused to remove the undesirable events and to increase the signal/noise ratio, without affecting the amplitude spectrum. We considered the Aki-Richards approach [2] in order to obtain as outputs the compressional- and shear-waves reflectivity sections. Comparing and manipulating the two sections, we could extract the following information: the main lithologic changes (lateral and vertical comparing the two sections), and the Poisson ratio contrast that is very useful to identify the aquifers. The AVO results allowed us to identify the main lithologic and fluid changes.

VELOCITY ANALYSIS

We reconstructed the aquifer depth structure by performing a tomographic inversion of the reflected arrivals. The adopted tomographic algorithm (CAT-3D), based on the SIRT method and the minimum-time ray tracing, can estimate the velocity field and the reflector structure in

sequence [3]. The model is a blocky one, with voxels (3D case) or pixels (2D case) where the velocity is assumed constant. The base and top of the pixels/voxels define the reflecting/refracting interfaces that may be curved and dipping interfaces. The tomographic algorithm is based on the iterative procedure shown in Figure 1. The procedure started from an initial model, generally with constant velocities within the layers and horizontally flat interfaces, and a set of interpreted events picked on the seismic data. In our case, the initial velocity model is obtained by the interpolation of the well data available in the study area. Using the wells' stratigraphy and some seismic sections of the italian CROP project (a project to identify the main geological structures of the Italian peninsula; [4,5,6,7]), we built a 3D multiparameter (P- and S-wave velocities, density and quality factor values of both P and S waves) seismic model, which shows the presence of gravel saturated layers alternated by clay impermeable layers (Table 1 and Figure 2, left).
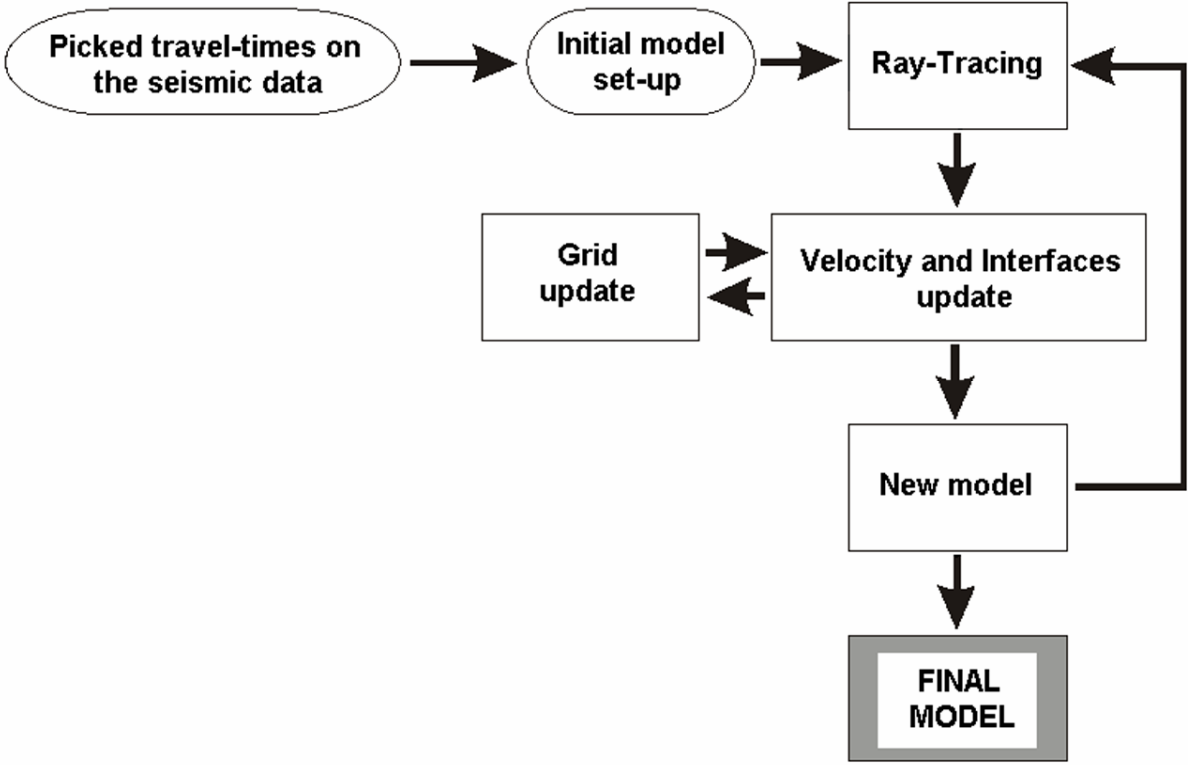
Figure 1. A flowchart of the travel-times tomography algorithm adopted.

Figure 2 (right) shows a synthetic shot obtained with the commercial software Tesseral, in which the velocity model is shown in the same Figure and the acquisition geometry is the same of the 2D line 2 here analysed (see the acquisition parameters in [1]). The synthetic data was (performed) used before the acquisition to determine the best acquisition to detect the main targets.

Table 1. Seismic properties of the aquifer model shown in Figure 2: compressional-wave (P) and shear-wave (S) velocities, density, and quality factors[5,6,7]. The seismic parameters of layer 6 (velocity and density) are linearly interpolated.

| Layer	Medium	V_P (m/s)	V_S (m/s)	ρ (kg/m^3)	Q_P	Q_S
1	Clay+gravel	1000	300	1700	20	20
2	Saturated gravel	1600	450	1900	40	40
3	Clay	1800	600	2000	30	30
4	Saturated gravel	2200	800	2100	50	50
5	Clay	2000	700	2200	40	40
6	Gravel+sand+clay (top)	1800	600	1900	60	60
6	Gravel+sand+clay (bottom)	2500	1000	2300	60	60
7	Carbonatic basement	3500	1900	2800	100	100
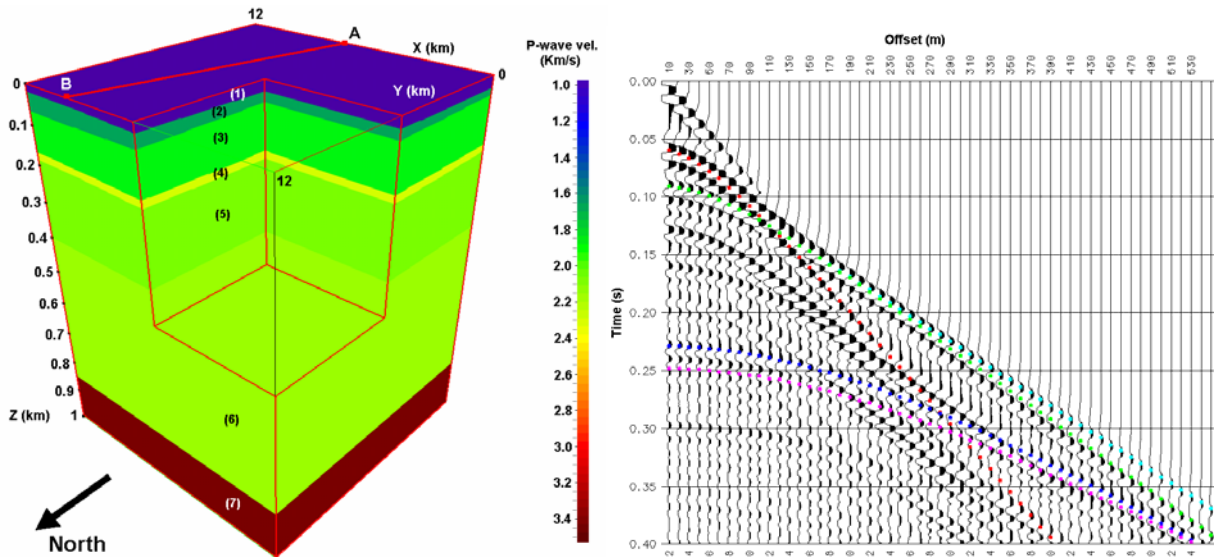
Figure 2. Left: 3D seismic model of the aquifer, whose seismic parameters are shown in Table 1. The seismic simulation was carried out along the line AB, which fits the 2D seismic survey here analysed (Line 2). Right: The synthetic seismogram of the first shot recorded at the surface: the vertical particle-velocity component is represented, and the dominant frequency is 80 Hz. The events of interest are the reflections of the second layer (red and green) and fourth layer (blue and purple), and the refraction of the second layer (sky-blue).

After the picking of the main reflectors, we invert the picked travel-times and update the model, until the variations of velocity and depth of interfaces become sufficiently small. The interface estimation follows the principle of minimum dispersion of the reflected (or refracted) points obtained from the estimated velocities. Within each single step, we can optimise the velocity grid by using an adaptive method for the grid updating (Figure 1). Reflected, refracted, direct waves and both P and S waves may be analysed by the package.

The compressional velocity field of the Line 2 were obtained inverting the travel time table of the main seven reflectors in the first 0.8 s (i.e about 700 m) because of the good quality of the data. In fact, the reflections were very evident from 0.03 s to about 1.1 s, while the refraction events were not always detectable because of velocity inversion caused by the alternance of saturated and unsaturated layers. The velocity fields clearly show the velocity inversion caused by the presence of the aquifers. A pre-stack depth migrations were performed in order to validate the tomographic velocity fields and obtain the real geometry of the structures.
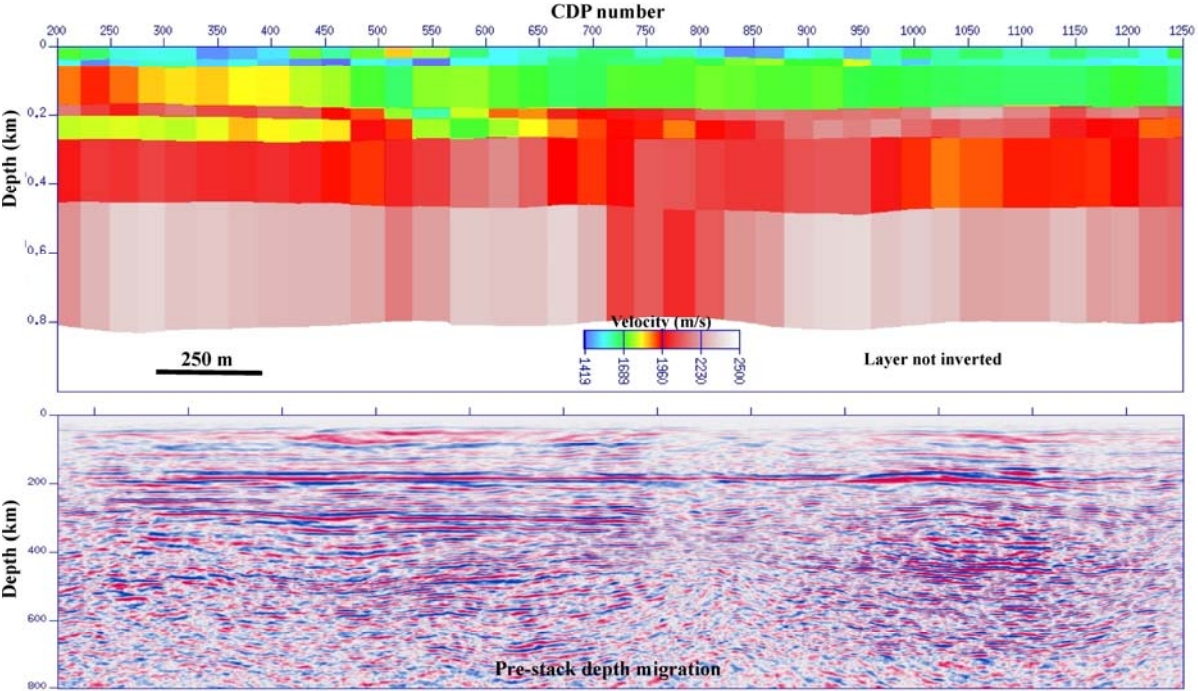

Figure 3. Top: velocity model obtained after the tomographic inversion. Bottom: pre-stack depth migration section.

Figure 3 shows the final velocity model obtained after the inversion procedure (top) and the pre-stack depth migration performed by using the so-obtained velocity field (bottom). The velocity model clearly identifies the shallow aquifer (at about 20 m depth) and the deeper aquifer (at about 200 m depth). Note the high velocity detected in the second aquifer in the right part of the line. Moreover, the satisfactory result(S) of the pre-stack depth migration validate the velocity model.

Finally, we produced new stacked sections by using the tomographic velocity, improving significantly the seismic imaging [1].

AMPLITUDE VERSUS OFFSET

The high-energy events evidenced in the seismic sections and the AVO effects in the shot domain (see as example Figure 4) can be associated either with lithologic changes or to the presence of fluids at elevated pressure. To better discriminate between these effects, we performed an amplitude variation versus offset analysis by using a commercial software

460

(GeoDepth$^{©}$; Paradigm Geophysical). We followed the Aki and Richards's [2] approach for the linearization of the Zoeppritz equations. This approach considers the linearization of the equations with respect to the P-wave velocity reflectivity (mainly influenced by the near offsets), the S-wave velocity reflectivity (mainly influenced by the medium offsets), and the density reflectivity (related to the very large offsets). The amplitude along each reflection is inverted by applying the Aki and Richards' procedure, and the variation of amplitude versus offset is translated in terms of P- and S-wave velocity reflectivity. After the AVO inversion, we obtain two sections in the time domain: the P- and S-wave reflectivity sections. Comparing the two sections, we can underline the main geological structures and the presence of fluid. In fact, comparing the P and S reflectivity sections, it is possible to discriminate between the reflections caused mainly by geological features and the reflections that can be attributed to fluid content variation.
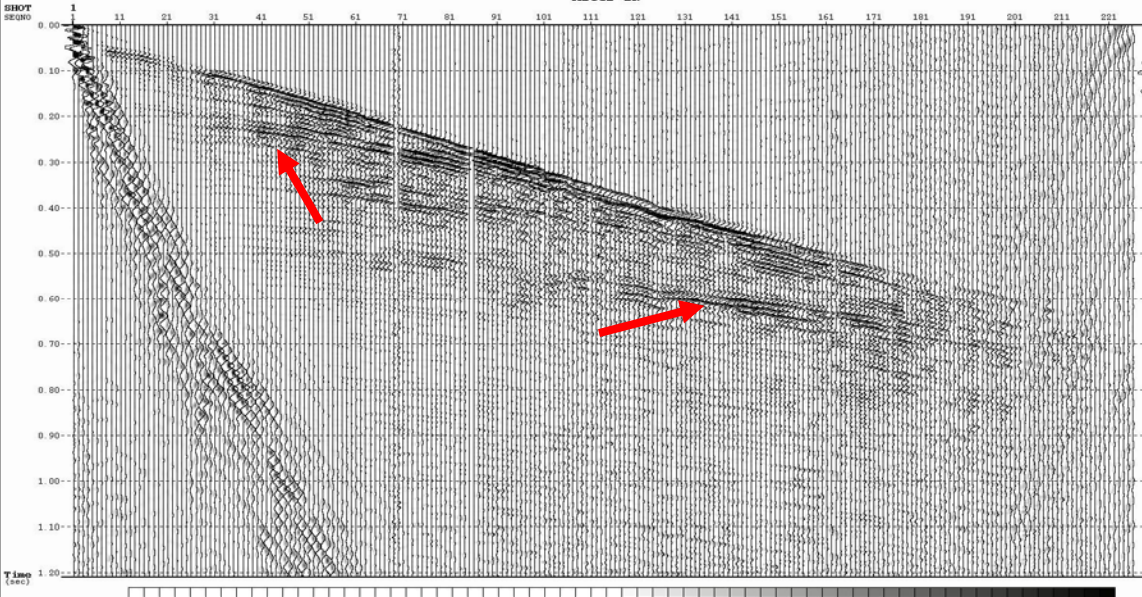
Figure 4. Example of AVO effects in the shot domain, as indicated by the red arrows.

The inputs of the amplitude inversion are (i) the data, processed following a true-amplitude scheme [1], (ii) the acquisition geometry, used to apply a correction for source and receiver directivities, (iii) the velocity model, obtained by tomographic inversion. The velocity model is used to calculate the ray path and translate the offsets in angles of incidence. We analysed the variation in the amplitude versus angle of incidence and obtained sections of both P- and S-wave velocity reflectivity, where the reflectivity is defined as the ratio between the variation of a parameter and the value of the parameter itself. For more details about the procedure see for example [8].
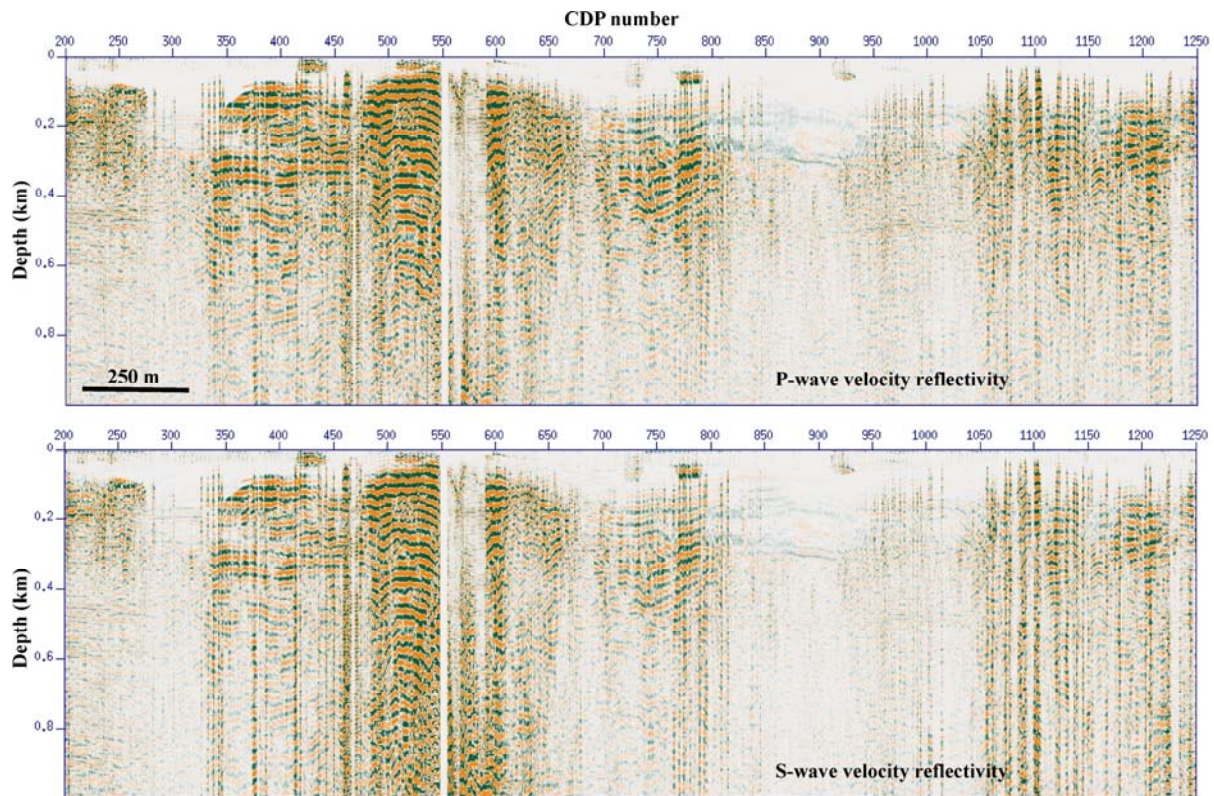
Figure 5. P- (top) and S-wave (bottom) reflectivity sections obtained after AVO inversion.

Figure 5 shows the P- and S-wave reflectivity sections after the AVO inversion. The two main aquifers are quite well identified in both sections confirming that the fluids are in overpressure condition.

To better interpret the AVO results, we evaluate the ratio between the P- and S-wave reflectivities, providing information about the Poisson ratio contrast (Figure 6, top). As expected, this AVO representation indicates that a strong Poisson ratio contrast is present across the two main aquifers. The red and white colours around the green part indicate that the limit of the reliability of the AVO inversion. Note also the high contrast at about 500 m depth, associate to a lithologic change.

Finally, we evaluate the crossplots between the P- and S-wave velocity reflectivities to verify if the main domain has different petrophysical characteristics. So, we selected two areas in which the two aquifers are well evidenced by the seismic data and the coverage is enough to guarantee a reasonable AVO inversion: between the CDPs 200 and 400 and between the CDPs 800 and 1000. Moreover, we consider different interval depth to detect different trends, as indicated in Figure 6 (bottom). The two selected zones produce similar results. In fact, the two main aquifers have different crossplot curves with respect to the other layers. The deepness, i.e. the relationship between P- and S-wave velocity contrasts, decreases versus depth, even if the characteristics of the layer between the two aquifers and below the second aquifer are very similar.
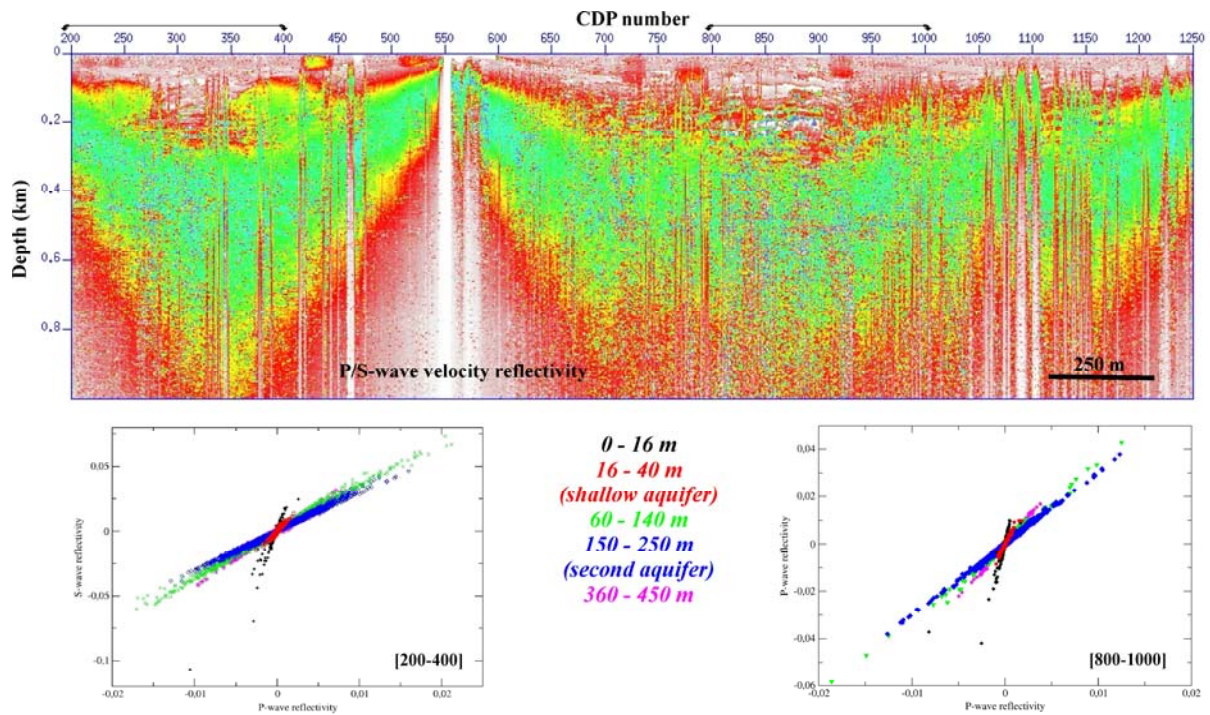
Figure 6. Top: P to S wave velocity reflectivity section; the lines indicate the area in which the crossplots are evaluated. Bottom: P- versus S-wave velocity reflectivities at selected CDP intervals (left: between CDPs 200 and 400; right: between CDPs 800 and 1000) and at selected depth: shallow part (between 0 and 16 m; black colour); across the first aquifer (between 16 and 40 m; red colour); between the two aquifer (between 60 and 140 m; green colour); across the second aquifer (between 150 and 250 m; blue colour) and below it (between 360 and 450 m; magenta colour).

DISCUSSIONS AND CONCLUSIONS

The non-conventional analysis applied to the 2D seismic line (tomographic velocity analyis and AVO) allowed us to characterize the petro-physical characteristics of the sub-soil across aquifers. The velocity field detected the velocity inversion at the bottom of the main aquifers and lateral velocity variation inside each layer. These results are in according with the available information and the seismic stacked sections obtained from seismic acquisition [1]. In fact the subsurface is characterised by strong lithologic variations.

The crossplot of the P- and S-wave velocity reflectivities reveals the presence of the shallow (until about 50 m) and the deeper parts with different trends. Some deviations can be recognised in proximity of the second main aquifer (at about 200 m depth).

In conclusion, the method used to seismic characterise the area has provided satisfactory results.

REFERENCES

[1] Giustiniani, M., Accaino, F., Del Negro, E., Tinivella, U., and Nieto Yabar, D., 2006: *The CAMI project: high-resolution seismic survey to study shallow aquifer.* In this book.

[2] Aki, K., and Richards, P.G., 1980: *Quantitative seismology: Theory and methods.* San Francisco: W.H. Freeman.

[3] Vesnaver, A. Böhm, G., Madrussani, G., Petersen, S., and Rossi, G.; 1999: *Tomographic imaging by reflected and refracted arrivals at the North Sea.* Geophysics, 64, 1852-1862.

[4] Nicolich, R., Della Vedova, B., Giustiniani and Fantoni, F.; 2004: *Carta del sottosuolo della Pianura Friulana.* Litografia Cartografica, Firenze.

[5] Prasad, A., and Meissner, G., 1992: *Attenuation mechanism in sands: Laboratory versus theoretical (Biot) data.* Geophysics, 57, 5, 710-719.

[6] Bourbié, T., Coussy, O., and Zinzner, B., 1987: *Acoustics of Porous Media*, Gulf Publishing, Houston, Texas, pp. 192,240.

[7] Schön, S., 1996: *Physical properties of rocks. Fundamentals and principles of petrophysics.* Vol 18. Pergamon.

[8] Accaino, F., Tinivella, U., Rossi, G., and Nicolich, R., 2005: *Geofluid evidence from analysis of deep crustal seismic data (Southern Tuscany, Italy).* Journal of Volcanology and Geothermal Research, 148, 46–59.

EVIDENCE OF CLIMATE CHANGES ON THE UPPER PLEISTOCENE AND HOLOCENE DEPOSITS OF THE VENICE LAGOON, ITALY

Luca Baradello[1], Luigi Tosi[2], Guiliano Brancolini[1], Ferica Rizzetto[2]

[1]Istituto Nazionale di Oceanografia e Geofisica Sperimentale, Trieste Italy, lbaradello@ogs.trieste.it
[2]Istituto per lo Studio della Dinamica delle Grandi Masse - CNR, Venezia

ABSTRACT

The effects of global climatic changes that occurred since the Last Glacial Maximum, are recognizable in the stratigraphic sequences from several areas in different locations around the world and, in particular, in coastal areas. Our study reports some examples from the Venice Lagoon (Italy) of the paleoclimatic change effects on the mineralogical composition and textural characteristics of clay and sand deposits, with emphasis on the stiff layer, locally called "caranto" at the Pleistocene–Holocene boundary and on cemented sand formations outcropping inside the northern lagoon and about 6 km off the southern littoral in the Adriatic Sea. A large amount of sedimentological and stratigraphical information, deriving from 18 boreholes made along the Venetian littoral and 10 throughout two salt marshes in the lagoon, is available for this study, which includes detailed geotechnical, mineralogical, geochemical, and textural data from more than 300 sediment samples. In order to correlate these data we performed High Resolution Seismic surveys inside and outside lagoon. Our HRS acquisition system consists of a boomer composed by an electro-dynamic transducer mounted on a catamaran frame. We collected data with bathymetry range 0.6 m to 15 m.

INTRODUCTION

The Venice Lagoon is located in the north-western Adriatic Sea and outlines an arch-shaped area of about 550 Km^2 bordered by a barrier island system seawards. Communication between lagoon and sea is guaranteed by three tidal inlets (Chioggia, Malamocco and Lido). Within the Venetian Upper Pleistocene-Holocene stratigraphic sequence some layers show diagenesis related to particular climatic conditions: the over-consolidated clay, locally known as "caranto", which is found at the Pleistocene-Holocene boundary; cemented sand outcropping inside the lagoon and off the southern littoral; a Late Holocene (Roman Times) high marsh event [5,6].

The deposits of the Late Pleistocene Lowstand System Tract (LST) are represented by alluvial sediments related to the Last Glacial Maximum (LGM); the upper layer (about 18kyr B.P.) is often characterized by pedogenetic process evidences, with the top marked by an unconformity which has an erosional character, and a hiatus covering a period between 7 and 10 kyr. The following Transgressive System Tract (TST) deposits were accumulated during the sea level rise beginning from about 9 kyr B.P. Landwards the TST bottom deposits are represented by fluvio-deltaic sediments related to flood processes, whereas seawards littoral and lagoon lithofacies, which accumulated during a stillstand phase of the transgressive event, are recognizable. The Highstand System Tract (HST) deposits that developed beginning from about 6 kyr B.P., are representative of the following seaward progradation phase: their accumulation was due to a high fluvial sediment supply, combined with a remarkable decrease of the sea level rise rate. As consequence a prograded barrier, composed of coast

parallel beach ridges, developed under wave-dominated littoral conditions and a wide lagoon originated in back-barrier position. Landwards the presence of alluvial and freshwater swamp lithofacies within the lagoon deposits gives evidence of deltaic bodies originated by ancient branches of the Piave and Brenta rivers, which flowed directly into the lagoon [5][6].
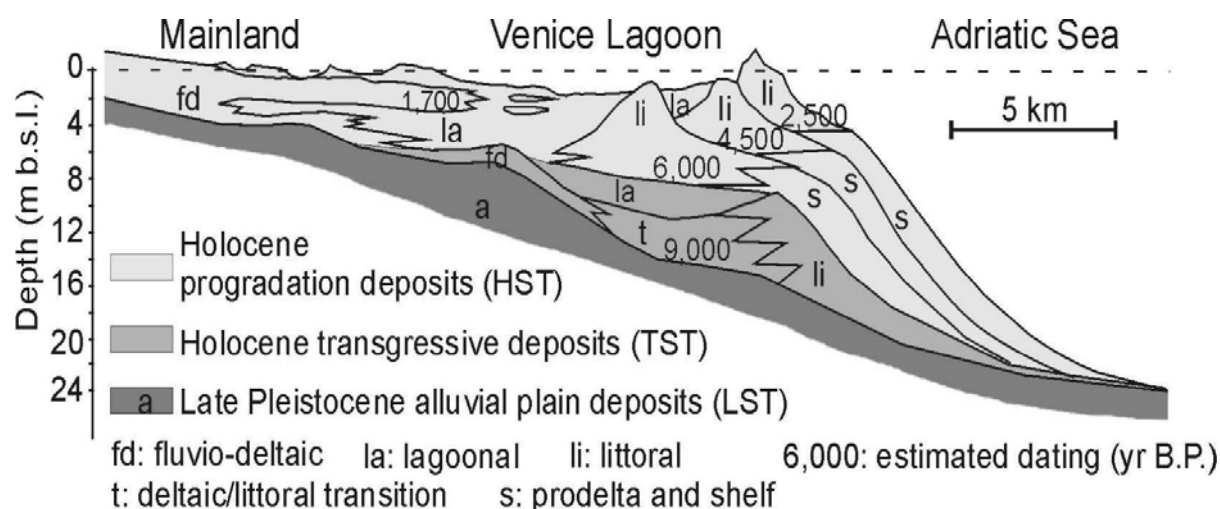

Figure 1. Simplified stratigraphic architecture and depositional environments of the Upper Pleistocene and Holocene of the Venice coastal area

METHODS AND MATERIALS

A large amount of mineralogical, sedimentological and stratigraphical information deriving from 18 boreholes taken along the Venetian littoral and 9 throughout two salt marshes in the lagoon was available [5][6]. To correlate all boreholes information we collected severals High Resolution Seismic (HRS) profiles with a boomer system [3].

This method utilizes a rapid water mass displacement produced by an electro-dynamic transducer (UWAK 05 by Nautik). The source is a piston moved by the electrical energy discharged from big capacitor realizing 150-450 Jouke/shot at 4kV (PULSAR 2002 by CEA). The piston is inside a plate mounted on a catamaran frame that allows the plate to be suspended at a constant depth of 30 cm, thus strongly reducing the dragging turbulences. The signals are collected with a preamplified oil-filled streamer (EG&G) composed by 8 piezoelectric elements (active section 2.8 meters) that have great sensitivity and large bandwidth. It's very important to keep the streamer as shallow as possible in order to avoid the destructive interferences between reflected signals and multiple events from air/water interface. This is not possible by increasing the boat speed because the noise increases. Then we can stick little floatings on cable. Usually the response of the streamers is much better than single hydrophone in water deeper than streamer length [3]. In fact the great advantage of the streamer is to increase the Signal/Noise ratio. On the contrary in shallow water every array produces spatial aliasing and can sum the signals in opposite phase, i.e. we could have spurious signals that mask real reflections. For this motive in very shallow water we don't use the classical geometry acquisition (source and streamer inline) but we apply a particular geometry: the streamer and the plate are towed on opposite sides (only lateral offset) behind the stern (figure 2). In this configuration we reduce a lot the array problems and we have good data (figure 5). The longitudinal offset is 2.5 meters. The optimum speed for this seismic

system is between 3 and 4 Knots. For the position we use navigation system interfaced a DGPS.

The acquisition card has a 24bit Sigma-Delta converter to improve signal dynamics. This seismic system has four principal advantages respect other VHR systems (air gun and sparkers): high peak of frequency and large bandwidth, good repeatability, directivity and portability [7].
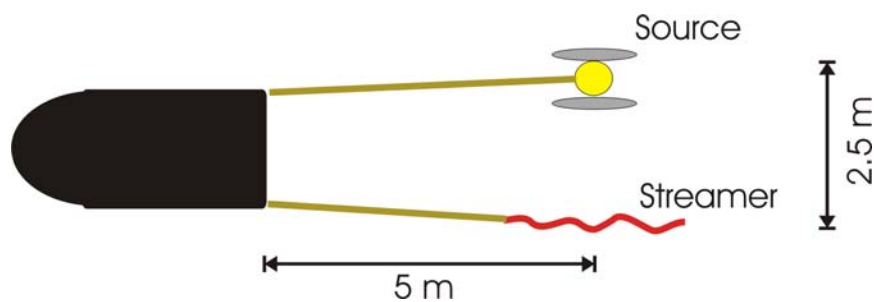
Figure 2. The acquisition geometry
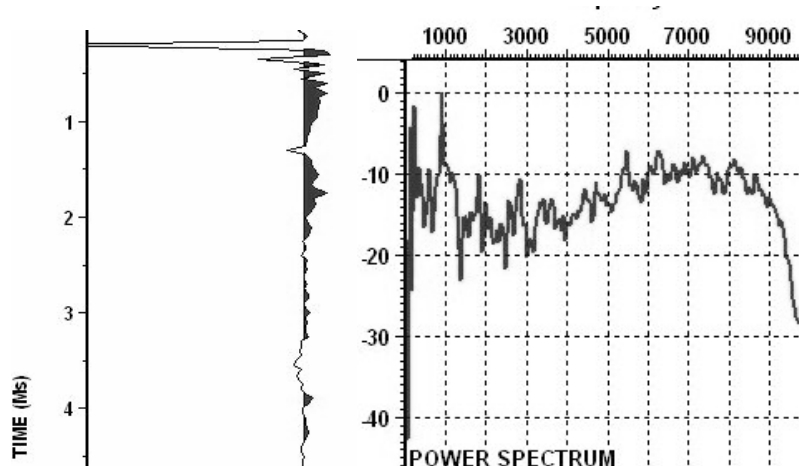
Figure 3. The boomer signature and power spectrum

RESULTS AND ANALYSIS

We focalised our attention on "caranto" layer [5][6]. This layer is rich in carbonate content at the bottom. From top to bottom we can observe a decrease of the clay mineral quantity and of the penetrometer resistance. The phyllosilicates exhibit a preferred orientation due to the over-consolidation process as evidenced by the highest penetrometer value; the LGM cold and dry climatic conditions and the prolonged exposure during the post glacial period favored the drainage that led to the over-consolidation of the sub-aerial clayey layers. The ^{18}O content of the carbonates in the "caranto" layer indicates precipitation under evaporating conditions of continental water. Authigenic barite (bright grains) and authigenic pyrite microcrystallites (bright grains < 2mm), growing along cracks in the sediment [2].

467
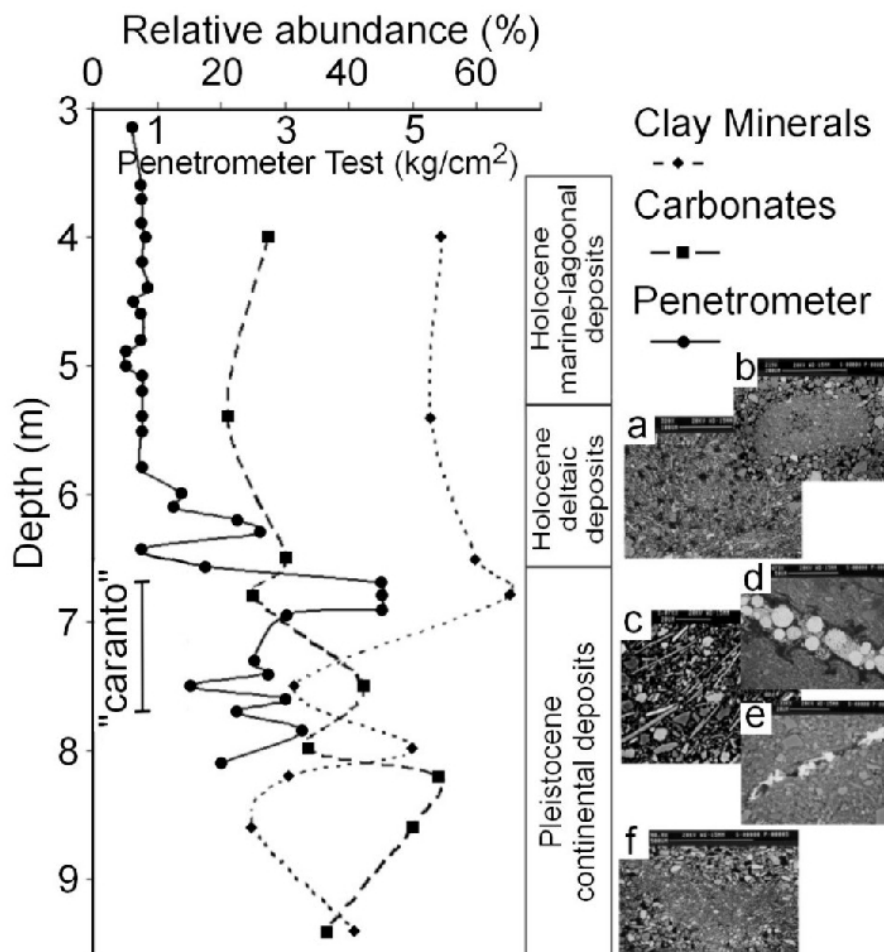
Figure 4. Mineralogical and textural characteristics of Late Pleistocene and Holocene clay layers. Photo a and b: elliptical lens of clay-size material within a poorly sorted, coarse-grained zone in an Early Holocene layer. Photo c: phyllosilicates exhibiting a preferred orientation; dark- to medium-gray grains are silicates; white grains, carbonates; elongated bright grains, chlorite; gray grains, mica; and black areas are pores. Authigenic barite, (Photo d) and authigenic pyrite microcrystallites (Photo e) growing along a crack in the sediment. Photo f: lens of clay-size material within a poorly sorted, coarse-grained zone in a sample below the "caranto" [2].

To create a map of "caranto" layer we carried out a great HRS survey on Venice Lagoon [1][5][6]. To overcame the logistic and technical problems in shallow water the HRS system has been implemented and installed in an ad hoc boat. We collected over 150 km of profiles inside and outside the navigation channel. In addition to "caranto" we detected many interesting geological-geomorphologic structures, i.e. paleoriver beds, ancient lagoon channels and shoreline ridges. To map all these features we have a research in progress within the Co.Ri.La. Project (3.16 Subproject).

In the Adriatic Sea 6 km off, in the HRS sections we found the cemented sand formations. Although these sands outcrop just at the emergence of the LST (Upper Pleistocene sequence), they appear to be related to the Holocene deposits. Their architecture is very complex, a lot of reflectors and fractures (figure 6).
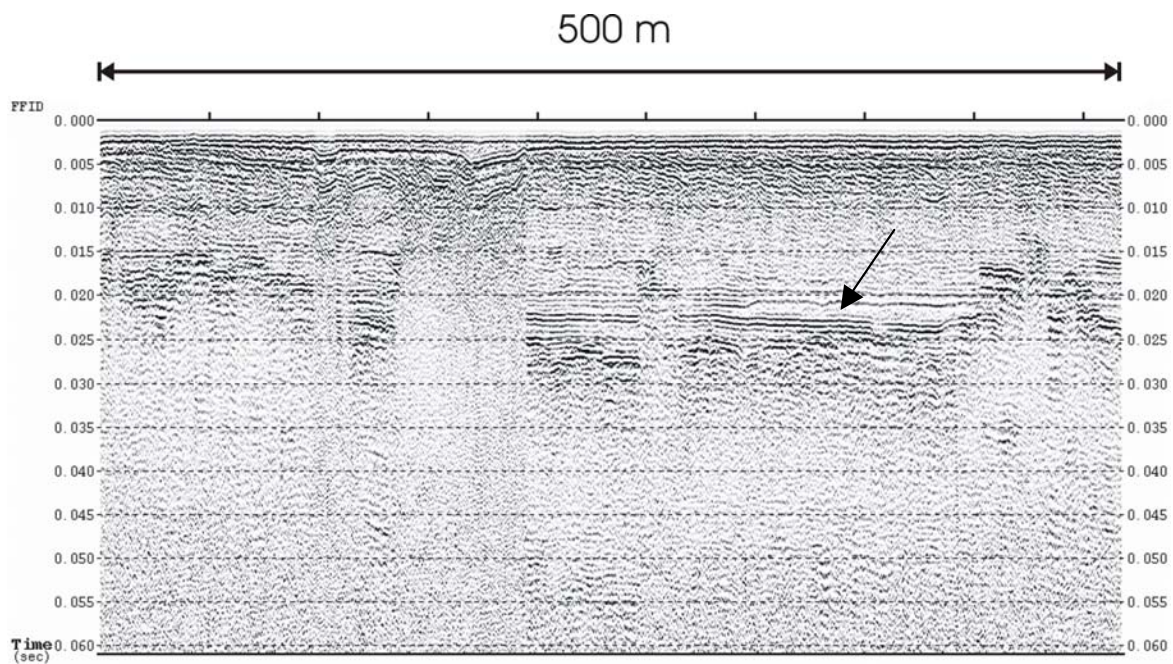
Figure 5. HRS profile in shallow water (~80 cm). The arrow indicates the "caranto" layer

Presently the diagenetic process is still debated, i.e. i) by carbonate mineral percolation through enhanced evaporation of seawater, ii) by fresh water seepage, ii) by methane seepage. Similar sand formations, like the beachrocks, are presently formed in tropical areas, then we can assume that the cemented sands found in the Lagoon of Venice were affected by a diagenetic process during Holocene "tropical-like" warm climatic events. Further investigation should be done to better understand this process and the age of these rocks.

CONCLUSIONS
This study has evidenced that the clay layers of the Upper Pleistocene and Holocene sedimentations present different diagenesis, i.e. variation in degrees of consolidation, in porosity, in textural and mineralogical characteristics, related to the original depositional environments and to the subsequent climatic changes. The sedimentological and stratigraphical information, deriving from boreholes, can have a good integration with HRS data. The boomer system is a good simple HRS method to detect and follow the subsurface substructures in shallow water too.
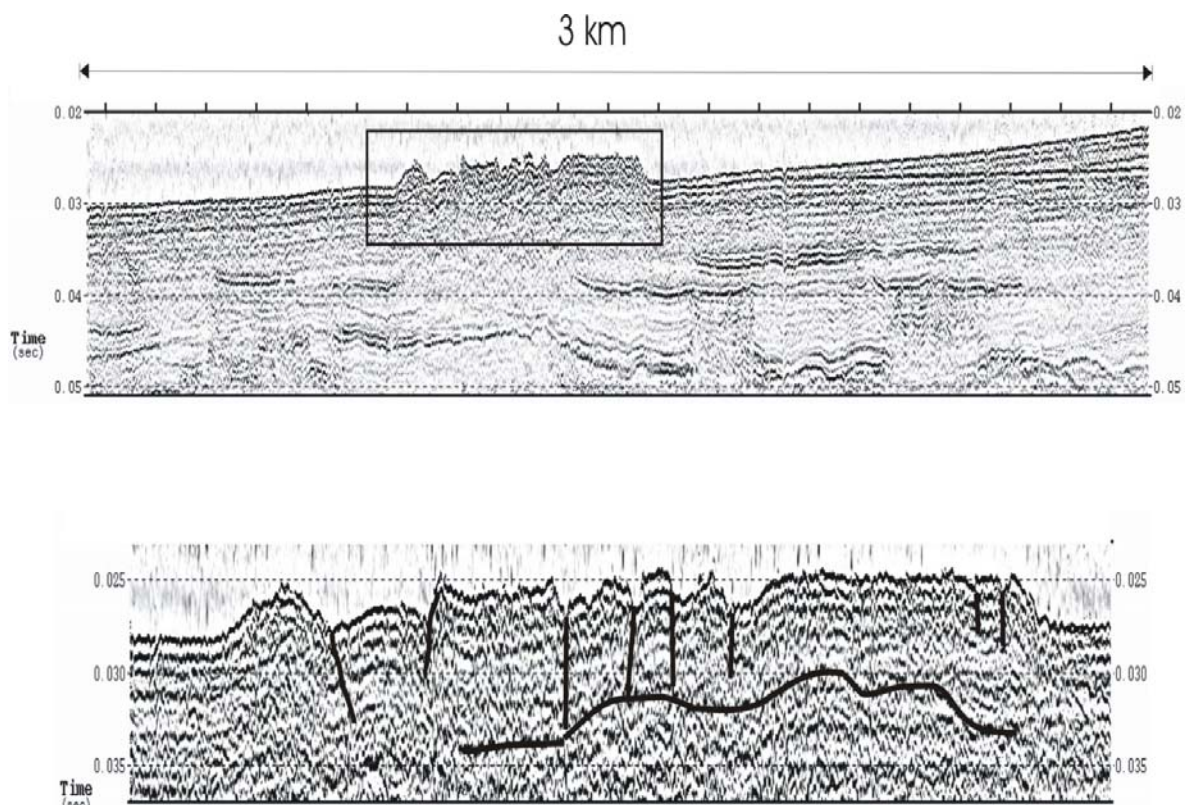
Figure 6. Above a HRS profile at 6 km off Venice Lagoon. Below a detail of the complex cemented structure showed in HRS profile. We can see a lot of fractures.

REFERENCES

[1] Brancolini G., Tosi L., Rizzetto F., Donda F., Baradello L., 2005. The unconformity at the Pleistocene-Holocene boundary in the Venice coastal area (Italy). Geoitalia 2005, Quinto Forum Italiano di Scienze della Terra, Spoleto, 21-23 settembre 2005, FIST, Epitome, 1, p. 253.

[2] Bonardi M., Tosi L., Rizzetto F., Brancolini G. & Baradello L. . (2006) - Effects of Climate Changes on the Upper Pleistocene and Holocene Sediment of the Venice Lagoon, Italy. Journal of Coastal Research, 39, pp. 279-284.

[3] McGee T.M., 2000: High-resolution seismic profiling on water. Annali di Geofisica, 43, 6, pp. 1045-1074

[4] Rizzetto F., Tosi L., Bonardi M., Serandrei Barbero R., Donnici S., Toffoletto F., 2005. The Geological Map of Italy: Map Sheets 128 "Venezia" and 148-149 "Chioggia-Malamocco". Geoitalia 2005, Quinto Forum Italiano di Scienze della Terra, Spoleto, 21-23 settembre 2005, Epitome, 1, pp. 70-71.

[5] Tosi L., Rizzetto F., Bonardi M., Donnici S., Serandrei Barbero R., Toffoletto F., 2006a. Note illustrative della Carta Geologica d'Italia alla scala 1:50.000. Foglio 128 – Venezia (in press).

[6] Tosi L., Rizzetto F., Bonardi M., Donnici S., Serandrei Barbero R., Toffoletto F., 2006b. Note illustrative della Carta Geologica d'Italia alla scala 1:50.000. Foglio 148-149 – Chioggia-Malamocco (in press).

[7] Verbeek N.H and McGee T.M., 1995: Characteristics of high-resolution marine reflection profile sources. J. Appl. Geophys., 33, pp. 251-269

DETECTING AND MAPPING SPRINGS INTO CLAY SOILS WITH GPR

Luca Baradello

Istituto Nazionale di Oceanografia e Geofisica Sperimentale, Trieste Italy (lbaradello@ogs.trieste.it)

ABSTRACT

Ground Penetrating Radar (GPR) is a fast no invasive and no destructive high-resolution geophysical technique for shallow investigations. During last twenty years GPR is used successfully to investigate and to map subsurface structures into several soil and to obtain high resolution imaging of the shallow sedimentary layers. These performances are well documented in literature.

In this work we used GPR method for detecting and mapping the subsuperficial springs in clay soils. The preliminary results are good because the radargrams show zones where the electromagnetic penetration is not possible (big clay thickness) and zones where there is the fresh water intrusion (clay and gravels mixed).

This acquisition is inserted to CAMI project, a LIFE - UE pilot project for studying with integrated methods the hydrographical district and to analyse the environmental impact of the human activities and their sustainability.

INTRODUCTION

In the last years the GPR method is widely employed in soil investigations and shallow subsurface mapping [4][5]. The GPR is composed by an antenna that emits the electromagnetic wave and then receive the echo produced by buried targets [2]. The electromagnetic penetration depends of conductivity of earth materials [1]. Wet materials like clay and loamy with water have higher losses while dry materials like sand and rock exhibit good penetration. The water content in soils influences strongly the GPR wave velocity, too. The phase velocity V is connected with dielectric real part constant ε by:

$$V = \frac{C}{\sqrt{\varepsilon}}$$

where *c* is electromagnetic velocity in vacuum

Since the water ε is 80, ten times the dry materials, its content in soil creates the anomalous zones of velocity.

Our goal is to apply GPR method to mapping the first few meters of the soil in the CAMI project. The first task of this project is create a aquifer model. We chose an area in North Italy (Friuli) where is located an important regional aquifer constituted by a thick pile of alluvial deposits (gravels, coarse sands and minor clay deposits). To create the geophysical model we integrated several geophysical investigations: Seismic [3] , ERT, Thermography, TDM and GPR.

ACQUISITION DATA

To collect data we used a georadar GSSI SIR2000 control unit equipped with a monostatic antenna, i.e. transmitter and receiver are the same dipole (zero-offset condition).
We chose to use 100 MHz instead of other frequency (400, 200 and 75 MHz) because for this clay soils this frequency has an optimum compromise between penetration and resolution [6].
In the study area we carried out the GPR profiles in continuous data collection method. In this case one person trails the radar along the line at constant velocity (normal walking) and the antenna transmits continuously the signals into the ground and records data while he fixes the marks.

During this fast acquisition we shot 32 pulses for second and marked manually every 5 meters. In the processing phase we made an interpolation of the data in X-direction on the basis of markers stored into headers data obtaining a new regular intertrace of 10 cm.
Other important processing phase is the time-zero drift correction. To detect the time-zero of the instrument we need to shoot the pulse against an obstacle in air at different known distances. Then in the Distance-Time graphic we calculate the intercepted line of the first arrival. This delay time is subtracted to all section.

Ursin [7] showed as the electromagnetic waves are very similar to seismic waves and then we can process GPR data with a classical seismic processing package adapted. The electromagnetic wave decays rapidly into the ground, to recover the signal amplitude we applied first a spherical divergence then we calculate the mean decay curve of all traces and we applied its inverse.

Finally a recursive bandpass butterworth filter with frequency range depending by depth was designed.

To determine the velocities field in our zero-offset profiles we used the hyperbola best fitting method. This method consists to individuate the strong diffractions apexes in the processed sections and to follow with a mathematical hyperbola the whole diffraction signal. The velocity of the media determined the hyperbola shape. For this area we average a radar velocity of 7-8 cm/ns.

In the study area we collected 10 km divided into 30 parallel profiles.

DATA INTERPRETATION

From the data observation we can divide the study area in two characteristics type of subsurfaces: A) zones with a incompact superficial layer over a compact layer of clay where the electromagnetic wave didn't have penetration (figure 1); B) zones with a mix gravels-clay where the GPR detect several structures (figure 2). Probably the B zones are characterized by subsuperficial fresh water flux and springs (figure 3).
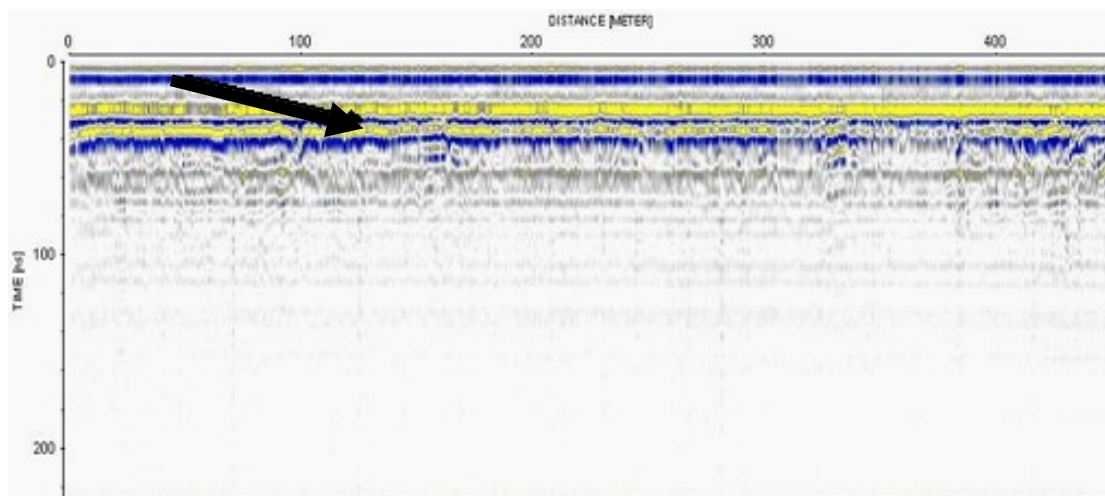
Figure 1. This GPR profile shows only the discontinuity (arrow) incompact-compact soil (classic zone A).
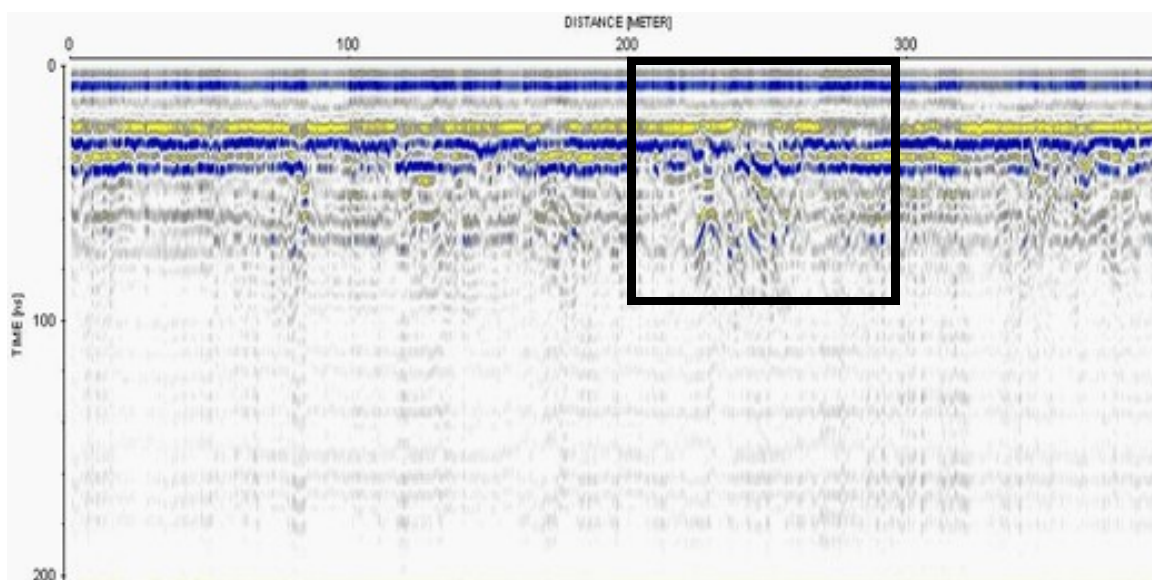
Figure 2. This GPR profile shows the zone where the electromagnetic waves have penetration and detect targets. (classic zone A).
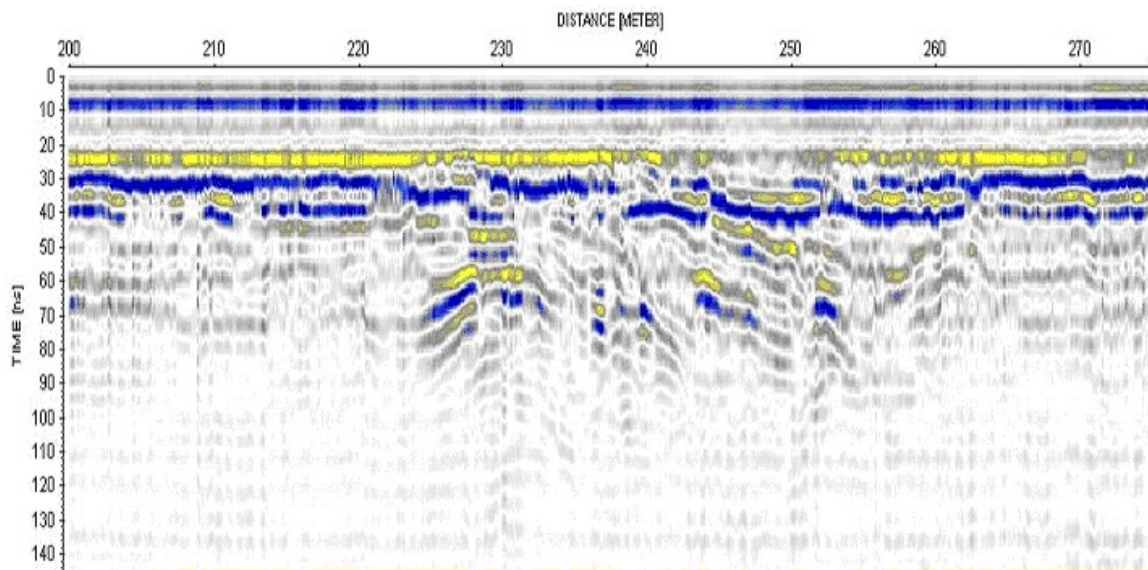
Figure 3. Detail of previous GPR profile. The visible structures are gravel where are springs.

CONCLUSIONS

In our study we saw that GPR is a useful method to characterize the first layers of the soil. We can discriminate where there are thick layers of clay (the electromagnetic waves don't go down) and where the clay is absent or mixed with gravel. In this second case the fresh water can create the springs. The next step will be to map these zones and to compare the GPR results with the Thermography analysis of area.

Acknowledgements
I wish to thank to Dr. Francesco Fanzutti and Mr. Alfio Barbagallo for the help in acquisition phase.

REFERENCES

[1] Daniels, D.J. (1996), Surface-Penetrating Radar BSc MSc Ceng MIEE MIEEE, pub. The Inst. of Electrical Engineering, London, UK.
[2] Davis, J.L., Annan, A.P. (1989), Ground-penetrating radar for high-resolution mapping of soil and rock stratigraphy. Geophysical Prospecting, vol. 37, pp. 531-551
[3] Giustiniani M., Accaino F, Affatato A., Del Negro E., Yabar D.G.N. (2005), Example of high-resolution seismic survey to study shallow aquifer. Proceedings 11th Annual Meeting EAGE-Environmental & Engineering Geophysics, Palermo, Sicily, Italy
[4] McMechan G.A., Gaynor G.C., Szerbiak R.B. (1997): Use of ground-penetrating radar for 3-D sedimentological characterization of clastic reservoir analogs. Geophysics, vol. 62, n. 3, pp. 786-796.
[5] Meschede, M., Asprion, U., Reicherter, K. (1997), Visualization of tectonic structures in shallow-depth high-resolution ground-penetrating radar (GPR) profiles. Terra Nova, vol. 9, n. 4, pp.167-170.

[6] Smith D.G., Jol H.M. (1995), Ground penetrating radar: antenna frequencies and maximum probable depths of penetration in Quaternary sediments. Journal of Applied Geophysics, vol. 33, n. 1-3, pp. 93-100.

[7] Ursin B. (1983), Review of elastic and electromagnetic wave propagation in horizontally layered media Geophysics, Volume 48, Issue 8, pp. 1063-1081.

THE PLACE NAMES REFERRING TO WETLANDS AS A KEY TO UNDERSTANDING HISTORICAL CHANGES OF THE MEDITERRANEAN WETLANDS. APPLICATION TO THE DOÑANA NATURAL PARK

Arturo Sousa[1], Julia Morales[1], Pablo García-Murillo[1], Leoncio García-Barrón[2] & Sukran Sahin[3]

[1]Department of Plant Biology and Ecology, University of Seville, Spain,
asousa@us.es;jmorales@us.es;pgarcia@us.es
[2] Department of Applied Physics II, University of Seville, Spain, leoncio@us.es
[3] Department of Landscape Architecture, Ankara University, Turkey, sahin@agri.ankara.edu.tr

ABSTRACT

Although there exist numerous studies that use place names to reconstruct old landscape changes, this type of approach has been frequently under dispute.

On the other hand, wetlands in Mediterranean areas have undergone an intense degradation and desiccation process during the last centuries, due to recent climatic changes, like post-*Little Ice Age* warming, and mainly due to anthropic activities. In this study we consider linking both issues, to analyse if recent changes in wetlands during the 19th and 20th century are reflected in the place names referring to wetlands.

We have chosen a Doñana Biosphere Reserve with a special importance for bird migration and renowned by its wetlands. In this study area we have reconstructed the evolution of its wetlands (brooks, lagoons and ravines) since the end of 19th century with the help of aerial photography, satellite images, fieldwork, microtopography analysis and historical documents.

By means of the comparison of the evolution of wetlands and their names we prove that place names referring to lagoons and brooks reflect the regression and desiccation of wetlands in Doñana Natural Park. We can even note changes in the desiccation rate linked to the effect of the end of *Little Ice Age* (end of 19th century) and later to the anthropic activity (changes in wetlands due to the introduction of eucalyptus monoculture forestry and irrigated land during the second half of 20th century).

Thus, we can conclude that place names referring to wetlands make an efficient tool to tracking the wetland desiccation process and noting the inhabitants' perception of this process. This methodology has been applied to a zone with a great ecological value, and in our opinion it could be applicable to other study areas within the Mediterranean basin.

INTRODUCTION

Pioneer studies in the analysis of the visual perception of landscapes point out how toponymy suggests variations in the spatial definition of landscapes [1]. There are also authors who consider that toponyms are of significant interest as referents in the paleoecological reconstruction of landscapes submitted to a high degree of transformation [2].

However, the documents ignoring the purely linguistic interpretation, so as to use toponyms as instruments for the reconstruction of historical environments, have been often criticised.

The critics arise, especially, from the lack of data for confirming hypotheses, which are sometimes daring and that become rather personal interpretations [3, 4]. This work is a contribution towards elucidating this controversy. It is a specific study that does not use place names referring to wetlands to visualize and recreate the evolution of wetlands in the study area, but rather the opposite. That is, historical changes of wetlands in the study area have been analysed using classic methodology, and then contrasted. Only when changes have been reconstructed from more-objective sources (and thus, not subject to interpretation) has their reflection in place names been studied. If a clear and quantifiable relationship is found, we can conclude that the place names referred to wetlands can be used as a key to understanding historical changes.

For this purpose, the west sector of the Doñana Natural Park was selected, which covers some 25,000 hectares within the homonymous Biosphere Reserve.

MATERIAL AND METHODS

Evolution of the wetlands in the area under study

In order to analyse the evolution of the surface covered by the lagoons and of the length of the brooks, after a field work, the situations in 1987, after 1956 and at the end of the XIXth Century (~1869) was mapped. This required the use of different sources of data, depending on the dates, as summarised in Table 1:

Table 1. Dates and sources of information used in the reconstruction of the wetlands

Method/Time Period	1987	1956	S. XIX (~ 1869)
Field work	Yes	-	
Aerial photographs	Yes	Yes	
Satellite images	Yes	-	
Forestry files	Yes	Yes	
Historical documents	-	Yes	Yes
Historical maps	-	-	Yes
Microrelief analyses	-	-	Yes

More precisely, the flights dated in 1956 (scale 1:33000) and 1987 (scale 1:20000) were used, along with the LANSAT-TM (1986), SPOT (1989) and LANSAT-TM (1990) satellite images. The analysed historical data were obtained from files and documentary sources (over 20) of the XVIth and XXth centuries, along with 49 deeds and forestry reports of the area under study (1932-1978) and more than 70 historical maps (XVIIIth through XXth centuries).

The above data were supplemented with a reconstruction of the microrelief based on the obtainment of topographic isolines approximately every 2 meters. For this purpose, the original contour lines at a 1:10000 scale (obtained from more than 650 topographic elevations) were interpolated, following the methodology developed in previous publications [5, 6]. The results were mapped at a 1:25000 scale by measuring the surface of the lagoons and the length of the brooks by means of a *PLANIX 5000* planimeter.

Evolution of the place names referring to wetlands in the study area

The main procedure used was the compilation of local place names on historical maps of the area dated between 1869 and 1987. The compilation was limited to maps for two reasons. On one hand, is the essential need to associate each term in space and time –so as to know the

date and area where the studied terms appeared and disappeared. On the other, in the Spanish territory, military maps are considerably more reliable than the rest (such as those of the Rural Land Registers).

For the quantitative analysis, seven maps were selected (dated between 1869 and 1987), which included most of the place-name terms over the period under study and whose scales were acceptably reliable and detailed (see Appendix 1). As a whole, 691 toponyms from the study area were compiled and analysed, 233 of them referred to wetlands.
Table 2 shows the classification of the toponyms performed on the basis of criteria in other studies on this subject [7]:

Table 2. Classification of place names used

- Natural.
- Animals.
* Animals
* Native animals of wetlands
- Plants
* Plants
* Plants perceived as native
- Wetlands
* Lagoons
* Brooks
* Other wetlands
- Forestry
* Pine-groves
* Eucalyptus groves
- Others.
- Artificial
- Route infrastructures
- Urban infrastructures
- Others.

As it has already been proved [7], this type of study does not allow to use the absolute number of toponym types, because the latter tend to be more and more numerous as time goes by. Therefore, from these maps, the number and percentage of each place-name type were determined following the classification summarised in Table 2.

RESULTS AND DISCUSSION

Evolution of the wetlands in the study area
Figure 1 shows, separately, the evolution of the length of the small coastal brooks and of the surface of the lagoons in the area under study (between the end of the XIXth century and the end of the XXth century):
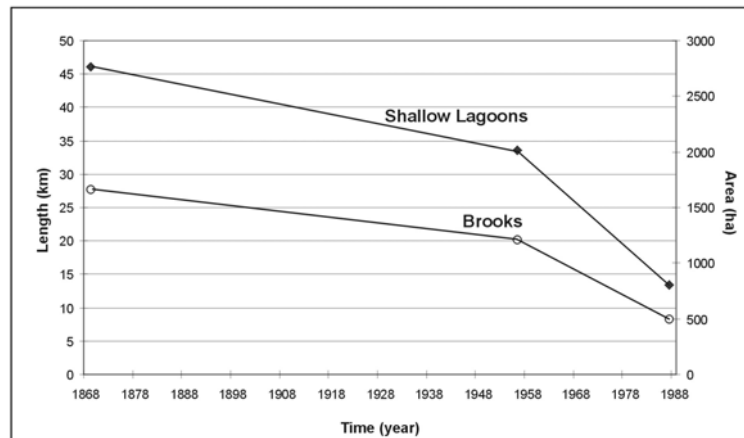
Figure 1. Regression of the small Atlantic coastal brooks and the shallow lagoons in the study area (1869 to 1987)

The results shown in Figure 1 evidence a clear reduction in both the length of the brooks and the surface of the lagoons in the Doñana Natural Park. This generalised regression of the wetlands in the study area coincides with the third and last humid peak of the *Little Ice Age*, dated at the end of the XIXth century for southern Spain [8], and at the 1830-1870 period in the Spanish Mediterranean coastal area [9]. Consequently, this desiccation is due, firstly, to the end of the *Little Ice Age* and, later on, during the second half of the XXth century, to an intensive reforestation process in the area [7] with fast-growing species (especially *Eucalyptus globulus* and *Eucalyptus camaldulensis*).

Evolution of the place names referring to wetlands in the study area
Table 3 shows the total number of toponyms analysed for each one of the dates studied, as well as the absolute number of the place names referring to wetlands for each one of the dates studied:

Table 3. Number and date of the place names shown on the maps. For year reference, see Appendix 1

Year of reference	1987	1981	1972	1947	1936	1897	1869
Total number of place names	184	123	89	116	91	47	41
Lagoons	31	28	21	23	17	21	5
Brooks	13	15	9	12	6	2	10
Other wetlands	6	4	3	3	5	4	7
Total wetlands	48	45	32	36	26	25	21

These results demonstrate that hydronyms, regardless their type, tend to grow in absolute numbers throughout time (as territories become better known and the maps are more and more detailed), in agreement with other studies on this subject [7].

Therefore, in order to visualise the tendencies of the various concrete types of toponyms, it is essential to calculated their percentage over the total number, as represented in Figure 2:
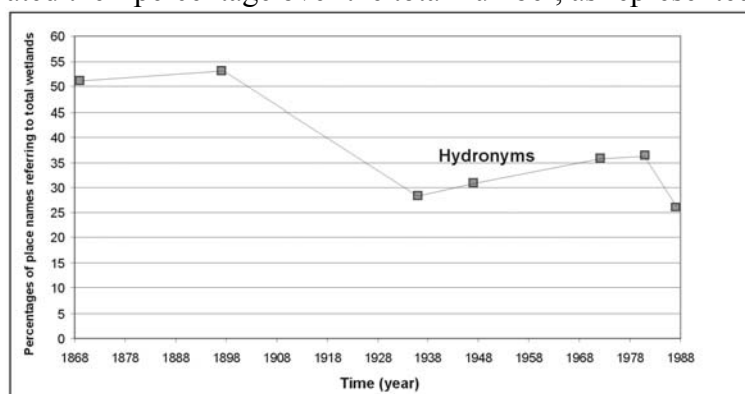

Figure 2. Evolution of the total place names referring to wetlands in the study area (1869 to 1987)

This figure reflects clearly the trend to decrease in the percentage of toponyms referring to the wetlands, for both brooks and lagoons (see Table 3).

The results demonstrate how the historical perception of the evolution of the wetlands in the study area can be followed up through a quantitative analysis of the toponyms referred to them. Consequently, these results confirm the possibility of using this tool as an indicator of the historical regression of the wetlands, same as previous studies have demonstrated the usefulness of this procedure in the follow up of changes in the vegetation cover, land use or territorial infrastructures.

This change in the wetlands, which coincides in time with changes in the Arctic lakes of Finland —named as *post-Little Ice Age warming* [10]—, would be the result of the post-XIXth century warming, in turn due to the summation of the termination of the *Little Ice Age* and the start of *Global Warming* [11]. These results are also coherent with the increase of the mean minimum temperatures detected in the study area by García Barrón (2002) and García-Barrón & Pita (2004). In the same way, it would be interesting to apply this methodology to eastern Mediterranean latitudes and to analyse whether the effects of recent climatic changes have been similar to those already found in the western Mediterranean regions.

REFERENCES

[1] Litton, R. B. (1968). Forest landscape. Description and inventories. *USDA Forest Services Research Paper PSW-49*. Berkeley, California.

[2] Alcázar, A., Martínez, A., Rey Benayas, J. M. & Ruiz, J. P. (1988). Toponimia y léxico relacionados con las descargas de aguas subterráneas en la cuenca del Duero. *Estudios Geográficos* 192: 329-339.

[3] Corominas, J. (1972). *Tópica Hespérica*. Gredos. Madrid.

[4] Rackham, O. (1986). *The History of the Countryside*. J. M. Dent. London.

[5] Sousa, A. & García-Murillo, P. (2002). Méthodologie pour l'étude des effets du *Petit Age Glaciaire* dans le Parc Naturel de Doñana (Huelva, Espagne). Essai de reconstitution des formations palustres et du drainage superficiel. *Publications de l'Association Internationale de Climatologie* 14: 359-367.

[6] Sousa, A. & García-Murillo, P. (2003). Changes in the Wetlands of Andalusia (Doñana Natural Park, SW Spain) at the End of the *Little Ice Age. Climatic Change* 58: 193-217.

[7] Sousa, A. & García-Murillo, P. (2001). Can place names be used as indicators of landscape changes?. Application to the Doñana Natural Park (Spain). *Landscape Ecology* 16: 391-406.

[8] Rodrigo, F. S., Esteban-Parra, M. J., Pozo-Vázquez, D. & Castro-Díez, Y. (1999). A 500 year precipitation record in Southern Spain. *International Journal of Climatology,* 19: 1233-1253.

[9] Barriendos, M. & Martín-Vide, J. (1998). Secular climatic oscillations as indicated by catastrophic floods in the Spanish mediterranean coastal area (14th-19th centuries). *Climatic Change* 38: 473-491.

[10] Sorvari, S., A. Korhola & Thompson, R. (2002). Lake diatom response to recent Arctic warming in Finnish Lapland. *Global Change Biology* 8: 171-181.

[11] Sousa, A.; García-Barrón, Morales, J. & García-Murillo, P. (2006). Post-*Little Ice Age* warming and desiccation of the continental wetlands of the aeolian sheet in the Huelva region (SW Spain). *Limnetica* 25: 57-70.

[12] García Barrón, L. (2002). Un modèle pour l'analyse de la sécheresse dans les climats méditerranéens. *Publications de l'Association Internationale de Climatologie* 14: 67-73.

[13] García-Barrón, L. & Pita, M. F. (2004). Stochastic análisis of time series of temperature in the south-west of the Iberian Peninsula. *Atmósfera* 17: 225-244.

APPENDIX 1.

Historical maps used for the quantitative analysis of the place names cited in Table 3 and Figure 2.

- 1869. *Huelva*. F. Coello.
- 1897. *Provincia de Huelva, nivelación*. Instituto Geográfico Estadístico. F. Noriega and J. Cobo del Guzmán. 1897-1900.
- 1936. *Mapa Geológico de España 1:50,000 y memoria explicativa*. Sheet 1.017 ("El Asperillo"). J. Gavala and Laborde. Ed. I.G.M.E.
- 1947. *Mapa Topográfico Nacional 1:50,000*. Sheet 1.000 (Moguer) and Sheet 1.017 ("El Picacho"). 1st ed.
- 1972. *Mapa Topográfico Nacional 1:50,000*. Sheet 1017 ("El Abalario"). 2nd ed. 1974. Instituto Geográfico y Catastral.
- 1981. *Cartografía Militar de España. 1:50,000*. Series L, Sheet 10-14 (1017) ("El Abalario"). 1981, 2nd ed. 1984. Sheet 10-41(1000) ("Moguer"). 1982, 2nd ed. 1988.
- 1987. *Mapa Topográfico de Andalucía, 1:10,000*. Ed. C.E.T.U., Junta de Andalucía. Sheets: 4-4, 3-3, 4-3, 3-1, 2-3, 2-1, 4-4, 2-4 and 2-2.

TEMPORAL ANALYSIS OF THE NORTH SEA-CASPIAN PATTERN INDEX (NCPI): a semi - empirical integration approach

Hasan Tatlı[1] and Yunus Borhan[2]

[1]Çanakkale Onsekiz Mart University, Faculty of Sciences and Arts, Department of Geography, 17020, Çanakkale Turkey, tatli@comu.edu.tr
[2] Technical University of Istanbul, Faculty of Aeronautics and Astronautics, Department of Meteorology, 34469, Istanbul, Turkey, borhan@itu.edu.tr

ABSTRACT

North Sea Caspian Pattern Index (NCPI) is identified by using the differences of the 500 hPa geopotential heights over the regions of the North Sea and Northern Caspian Sea. It is a teleconnection pattern associated with anomalous weather patterns in the Eastern Mediterranean, Eastern Europe, Anatolian Peninsula and Middle East. However, the spectrum of the NCPI shows that there is not a determining quantified spectrum embedded in it. Accordingly, the temporal characteristics of the NCPI are investigated with a new proposed semi-empirical method. At the first step, NCPI is integrated through the time when its integrand reaches to a restriction point of steady state. In the second step, the significant empirical orthogonal function (EOF) of the surface air temperature series in the windowing of 20-50°E and 30-60°N longitudes-latitudes is computed from the National Centers for Environmental Prediction – National Center for Atmospheric Research Reanalysis data sets. Similar to the integration of the NCPI, at the each of the steps, the empirical orthogonal function extracted from the surface air temperature series data set is firstly standardized and later it is integrated until its integrand matches a point of steady-state. Finally, it is noticed that the Fourier spectrum density, and also the Hilbert spectrum, of both of the time evaluation of the NCPI and EOF show interrelation temporal characteristics, are interpreted readily by the proposed semi-empirical approach.

Keywords: Empirical orthogonal function, Hilbert spectrum, integration, North Sea Caspian Pattern Index, spectrum density, surface air temperature

INTRODUCTION

The atmospheric correlations are crucial to understanding of short and long-term variability in climate. The most significant correlations are recognized as teleconnection patterns. However, these types of correlations do not really represent well-known traditional states of the atmosphere. In the frame of physical states of the atmosphere, one of very important variable among atmospheric variables is the air pressure. Air pressure patterns relate the tracks of dynamical effects near the surface do not involve body forces but survey surface weather systems. The principal way to validate the teleconnection relations involves spatial differences of semi-steady pressure centers (low and/or high) performing correlation with respect to climate variables; temperature and precipitation are such examples among climate variables. Hence, teleconnections are interested in summarizing climate variability.

One of the well-known teleconnection is the North Atlantic Oscillation (NAO) which dictates the exchange of the atmospheric mass between the Greenland/Iceland and the regions of

North Atlantic Ocean between the *35-40°N* latitudes, and it is characterized by a north-south dipole [2, 11, 12]. Since NAO occurs over Atlantic Ocean (*i.e.* water), the physical domain of the NAO is less friction comparable to the occurrence regions of the North Sea Caspian Pattern (NCP), this is the main reason that Kutiel and Benaroch [5] did not extract NCP Index near surface, but at 500 hPa level by using geopotential height differences in order to eliminate the local surface friction effects. However, the NCPI is more fluctuated than to the NAO Index. Although the NCPI shows noisy characteristics, some researchers found significant correlated structures between some of climate variables and NCPI [1, 5, 6, 7].

In this study, a semi-empirical method is proposed to extract steady-state properties of the NCPI associated with surface air temperature series which are in window of 20-50°E and 30-60°N longitudes-latitudes. The proposed method is based on integration of the NCPI through the time by the way of simply summation through the time after standardized it at each step before integrating, which is named as "Total NCPI" in this study. On the other hand, synoptic processes impose their spatial scales not only on changes with characteristic time of several days but also on month-to-month, year-to-year, and larger climatic changes, because temporal averaging preserves the spatial structure of the processes' features. In other words, if there is a long term anomaly of some climatic parameter, this anomaly has a horizontal size comparable with the characteristic size of cyclones and anticyclones. Therefore, integration of standardized index can also keep the index structure properties, but having a temporal averaging.

This paper includes the following aspects: in Section 2 the methodology and results are given. Some comments and conclusions are given in Section 3.

APPLICATION AND RESULTS

The starting point of this study of the impact of summarized of the NCPI's features on local to regional scales may be casted as regional climate variability of surface air temperature series. Regarding to Kutiel and Benaroch [5], NCPI has influences on surface air temperature series. Therefore, surface air temperature series are selected from NCEP/NCAR reanalysis data sets [3, 4] over the regions where we can not gather the risk of overlapping areas inferred from the thermal effects associated with the Siberian high. Accordingly, we can not escape from the influence of the Siberian high, but the area covered by 20-50°E longitudes and 30-60°N latitudes may be selected subjectively for the application example.

The data of NCPI is selected according to Kutiel and Benaroch [5] for 1958-2000 interval. In order to detect the significant evaluation; firstly, Fourier analysis is employed to the NCPI, and latter the NCPI is transformed to its analytical signal by aid of employing Hilbert transformation. Let us represent NCPI by *x(t)* and its analytical signal by *z(t)* then Hilbert transformation is obtained as in the following.

$$h(t) = \frac{1}{\pi} P \int_{-\infty}^{+\infty} \frac{x(t')}{t - t'} dt'$$

(1)

where *P* indicates the Cauchy principal value (for details refer to [8, 9]), and then the analytic signal *z(t)* is obtained as:

$$z(t) = x(t) + ih(t) = a(t)e^{i\theta(t)} \tag{2}$$

Herein *a(t)* represents the amplitude and $\theta(t)$ is the phase angle of the signal respectively, which are defined as:

$$\theta(t) = \tan^{-1}\left(\frac{h(t)}{x(t)}\right) \tag{3}$$

Additionally, the instantaneous frequencies of the signal are computed as in the following, but the phase angles should be first unwrapped, latter taking its derivative gives the instantaneous frequencies.

$$w(t) = \frac{d\theta(t)}{dt} \tag{4}$$

Taking integration with respect time of any signal is named as *total* thereafter; such as "1st total NCPI" represents the first integrated of the NCPI with respect time. Integration operator is indeed a linear operator, inverse of derivative operation. On the other hand, taking integration of any signal brings no misinterpretation; inversely, however during the taking derivative at each step of derivative we loose the high frequency component in the signal. Let us explain what we mean with a numerical example. If we have *N* number of discrete values (time series) with the time interval for $t = m\Delta t$ *(m = 0, 1, 2... N-1)* then we can represent this signal as:

$$x_m = x(m\Delta t) \quad m = 0,1,2,...,N-1 \tag{5}$$

Reconstruction the signal *x(t)* with the finite Fourier parameters can be written as:

$$\tilde{x}(t) = \frac{A_0}{2} + \left[\sum_{k=1}^{N/2-1} A_k \cos\frac{2\pi kt}{N\Delta t} + B_k \sin\frac{2\pi kt}{N\Delta t}\right] + \frac{A_{N/2}}{2}\cos\frac{2\pi(N/2)t}{N\Delta t} \tag{6}$$

If we now take derivative with respect time of the above signal, then we have

$$\&_m = \left(\frac{d\tilde{x}}{dt}\right)_{t=m\Delta t} = \frac{2\pi}{N\Delta t}\sum_{k=1}^{N/2-1} k\left[-A_k \sin\frac{2\pi km}{N} + B_k \cos\frac{2\pi km}{N}\right] \tag{7}$$

where the derivative of the last term in the Eq.6 was obviously disappeared. Since the NCPI has high frequency components, integration of a tabular data with high frequencies by using with one of numerical or Fourier integration methods give misinterpretation results of which are not desired. Instead of employing one of numerical integration methods, we simply apply summation operator to the signal above (cumulatively) after the signal is standardized (zero

485

mean and variance one). Inversely, instead of taking derivative; the time difference of the tabular data might now give exact results. After employing the proposed approach to the NCPI we have the results given in Figure 1. According to this figure, NCPI reaches a steady-state point at the *5th* iteration; and at the steady-state form, NCPI is now readily interpreted with very simple sinusoidal like signal.

If we now investigate mono-component temporal changes by plotted spectrum densities of the NCPI with respect to taking integration then we have the frequency spectra of totals of the NCPI as plotted in Figure 2. If we examine this figure closely, then it can be noticed that the spectrum densities are not significantly changed after the 2nd Total NCPI extracted which might lead to misinterpret the signals given in Figure 1.
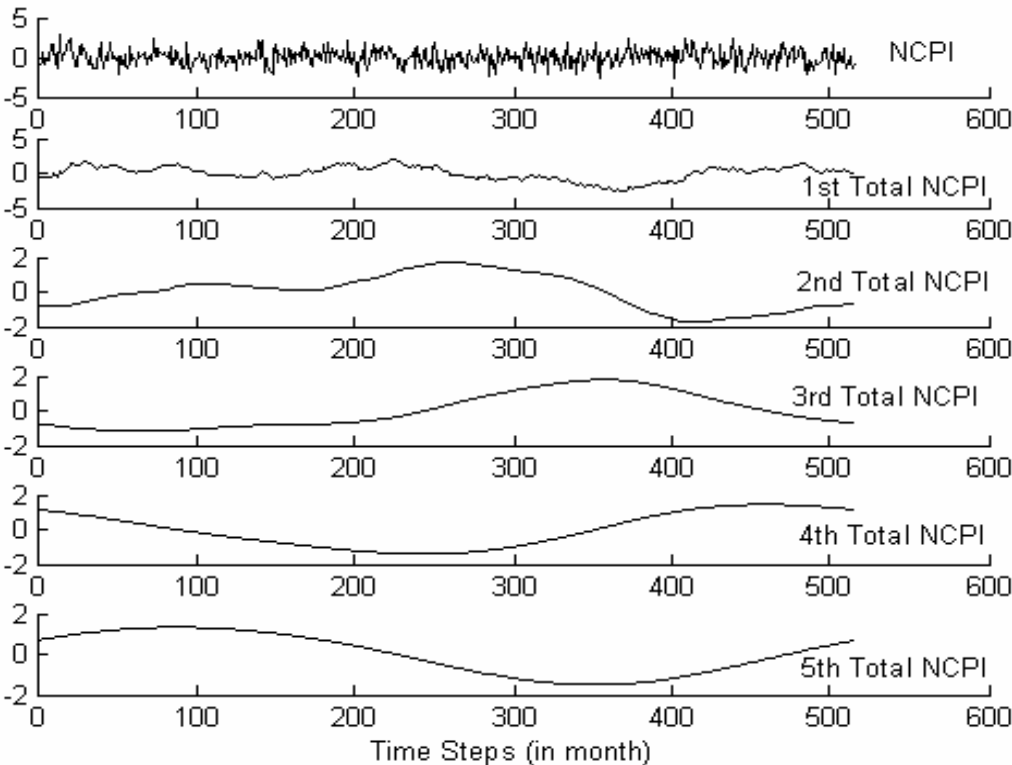
Figure 1. Time evaluations of the NCPI and its Totals with respect to time interval of months: "1st, 2nd … Total NCPI" abbreviations indicate the "first, second … integrations" of the NCPI.

In words, the spectral densities given in Figure 2 can not represent the time evaluation of totals of the NCPI. Hence, the instantaneous frequencies of the NCPI may have meaningful changes; as result of this opinion the Hilbert spectrums of the Total NCPI are extracted as shown in Figure 3.

If we compare the spectrums shown in Figure 3 with the results given in Figure 2, we have a suggestion that the Hilbert spectrum representation is more appropriate than to apply Fourier analysis. As seen in Figure 3, the shape of the spectrums are not significantly changed after *4th Total NCPI*, of which is consistent with nature of time evaluations of the NCPI explored

in Figure 1, with a restriction to reach a steady-state attraction. Consequently, there is consensus that the NCPI relates surface climate or flux variables regarding to [1, 5, 6, 7]. These authors found out the inter-correlated structures between NCPI and related variables based on the time evaluation month-to month or seasonal (*e.g.* winter). However, in this study, the inter-correlated structures are not divided into discrete months or seasons, besides it is thought and investigated in order to pronounce it in a total or continuum frame.

(a)

(b)

(c)

(d)

(e)

(f)
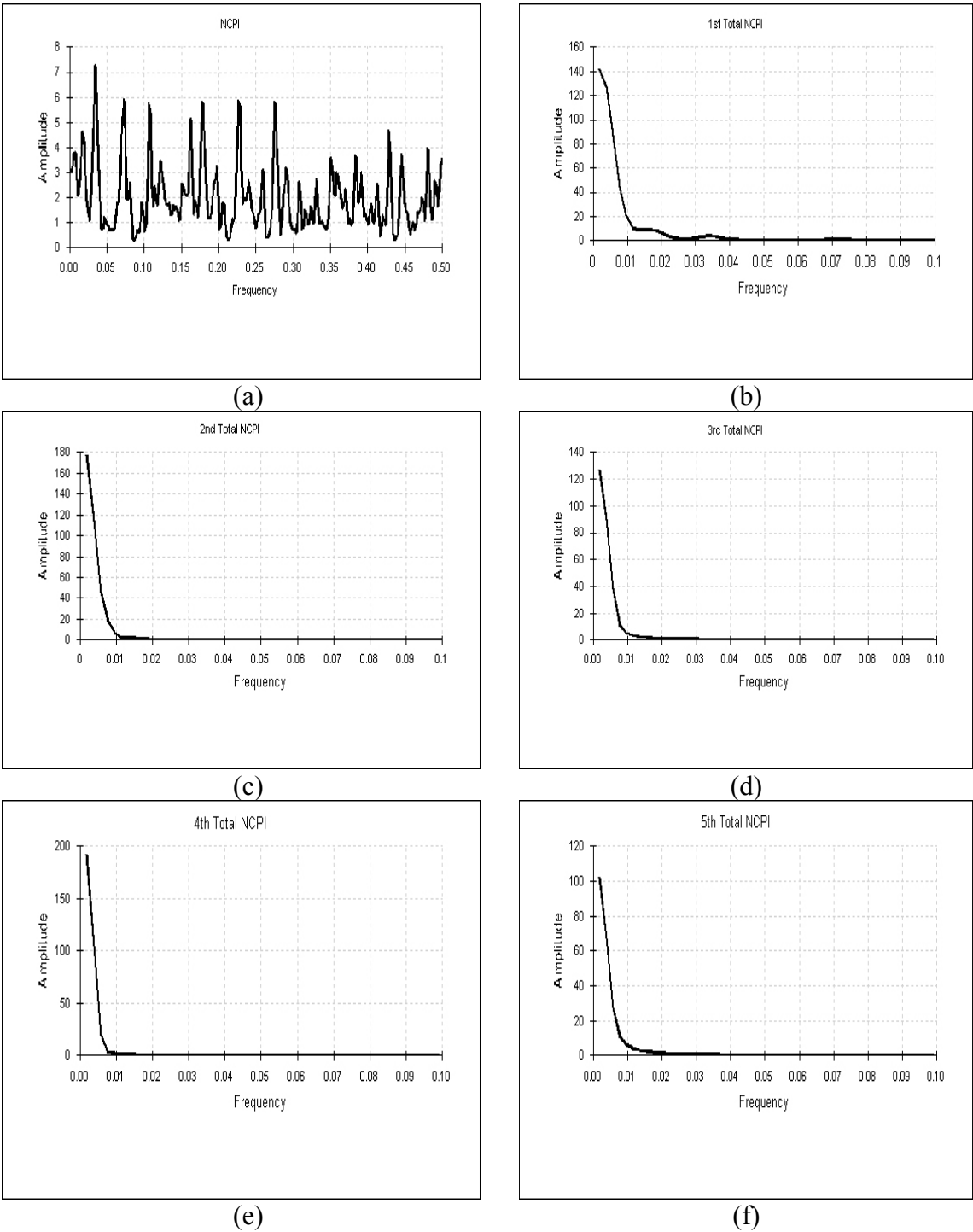
Figure 2. Fourier spectral densities of the NCPI and its Totals

Finally, employing Principal Component Analysis (PCA) to the surface air temperature series over the region of 30-60°N and 20-50°E, we have the results with the explained variances of each of the EOFs specified in Table 1, using multivariate techniques of Singular Value Decomposition (SVD) key method [10]. Accordingly, principal components which are also called Empirical Orthogonal Functions (EOF) in Atmospheric Sciences are employed in this study.

(a)   (b)

(c)   (d)

(e)   (f)
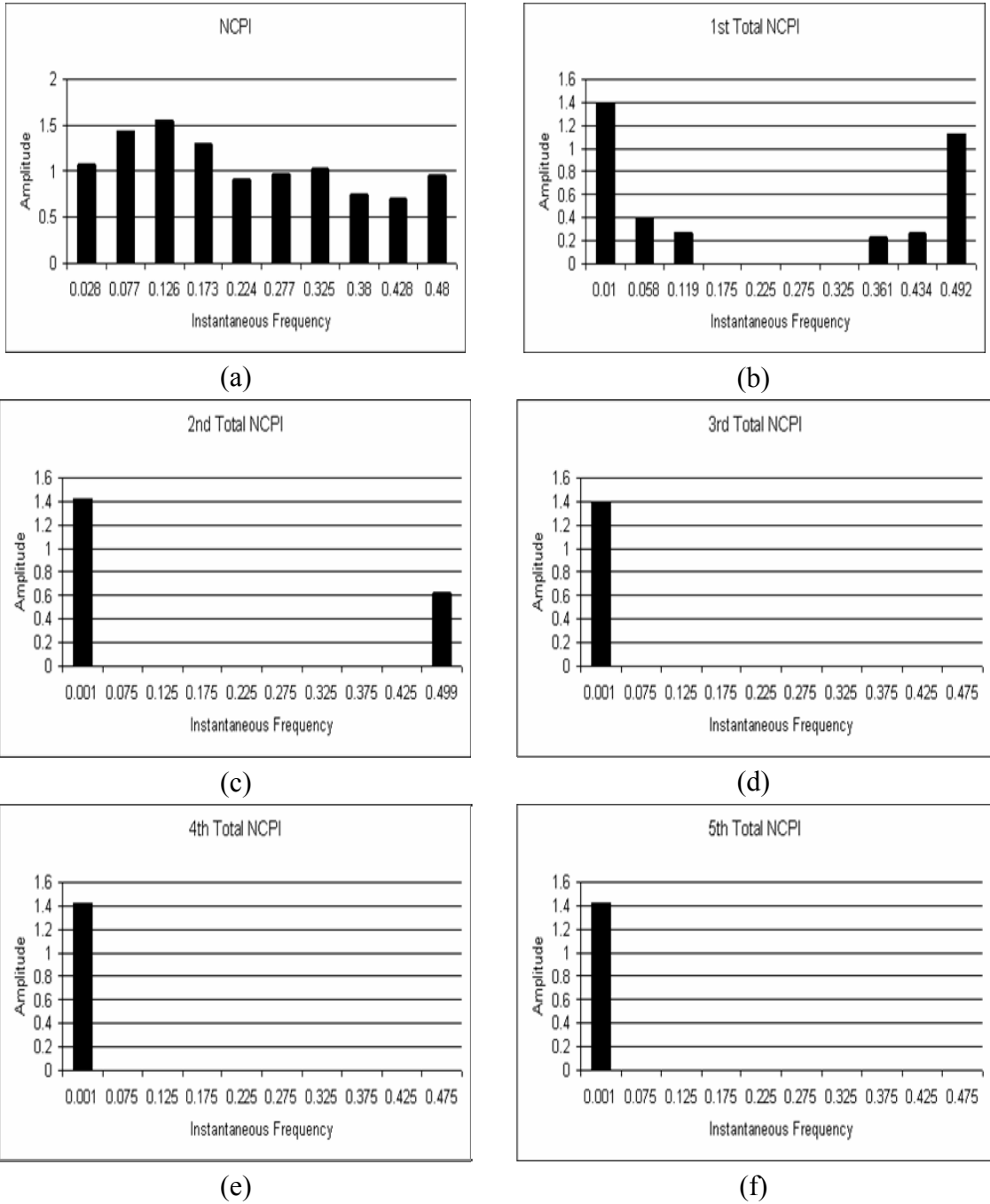
Figure 3. Hilbert amplitude line spectrums of the NCPI and its Totals: the horizontal axis is not in traditional known mono-component frequency, in classified disparate instantaneous frequency

According to the Table 1, the first EOF is significantly explained around 96% ratio to the total variance in the field of the surface air temperature variability. For this reason, the first EOF is selected on behalf of the surface air temperature variability. The same proposed integration method explained above is employed to the first EOF of the surface air temperature series, and the results arranged in Figure 4, are extracted.

DISCUSSION AND CONCLUSIONS

A semi-empirical method is proposed to revise the relationship of two representation field of the NCPI and surface temperature series with respect to their time evaluations. The method could identify similar evaluation, especially after 2nd order integration for both of the NCPI and EOF of the surface air temperature series. Interestingly, these similarities show low variability, and information content may be pending from the same kinship (or affinity) with respect to low time resolution (temporal averaging), could be inferred.

The results from the study of EOF of the surface air temperature results are presented in a similar fashion to the NCPI, except that in each case we show integrated patterns from the two fields which are optimized for the maximum linked temporal shapes with Fourier spectra and Hilbert amplitude spectrum (intends for instantaneous frequencies). However, from the physics of fluid dynamics; high order derivatives (or integration) may not have physical meaning with admiration of the real states of the atmosphere; unlike NCPI like signals are not intended to confirm the real states of the atmosphere, just summarizing climate variability. Based upon this approach, integration infinitely with respect to time might match a sinusoidal like signal which can be mentioned as temporal averaging, or low frequency oscillation in place of the natural properties of the real states of the atmosphere.
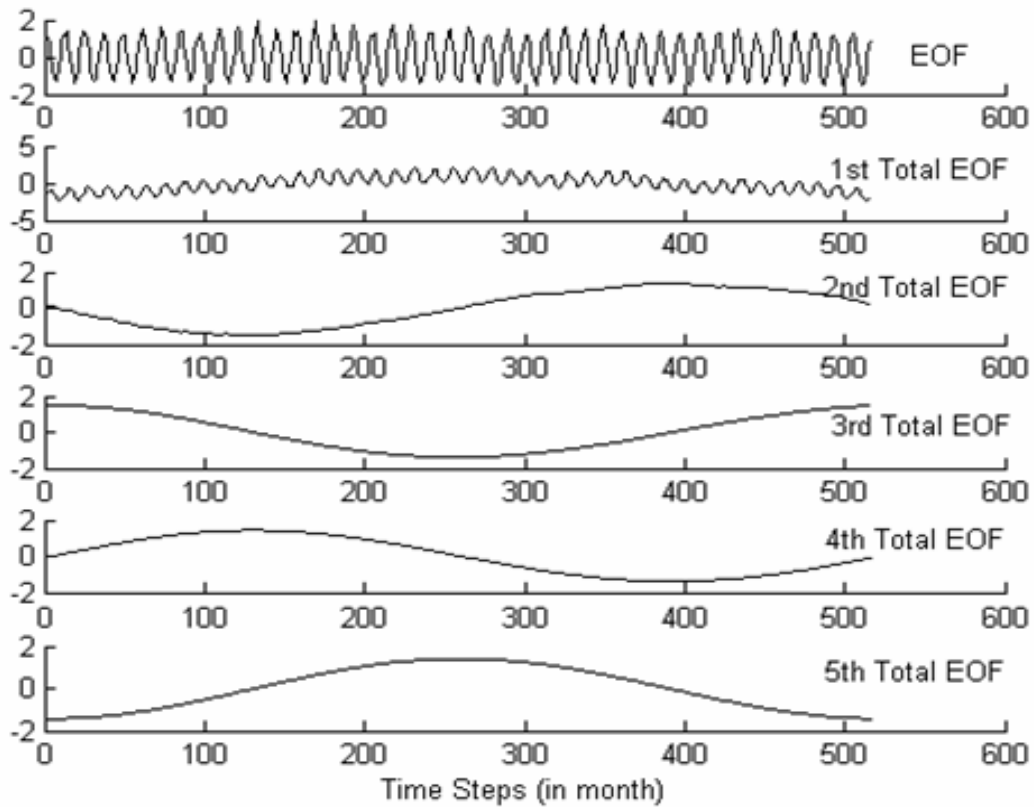
Figure 4. Time evaluations of the first EOF of the surface air temperature series in the range of 20-50°E and 30-60°N longitudes-latitudes: "1st, 2nd … Total NCPI" abbreviations indicate the "first, second …integrations" of the EOF as given in Figure 1

Table 1. Extracted EOFs of the surface air temperature series over the region of *20-50°E* and *30-60°N* with their explained variances

EOF	Explained Variance (%)	Sum of Explained Variance (%)
1	96.16	96.16
2	1.43	97.59
3	0.85	98.44
4	0.33	98.77
5	0.28	99.05
6	0.22	99.27
7	0.14	99.41
8	0.08	99.49
9	0.07	99.56
10	0.06	99.62

REFERENCES

1. Gunduz M, Ozsoy E. 2005. Effects of the North Sea Caspian pattern on surface fluxes of Euro-Asian-Mediterranean seas. *Geophysical Research Letters* **32**:1.4.
2. Hurrell JW, Hoerling MP, Phillips AS. 2004. Twentieth century North Atlantic climate change. Part 1: assessing determinism. *Climate Dynamics* **23**:371-389.
3. Kalnay E, Kanamitsu M, Kistler R, Collins W, Deaven D, Gandin L, Iredell M, Saha S, White G, Woollen J, Zhu Y, Chelliah M, Ebisuzaki W, Higgins W, Janowiak J, Mo KC, Ropelewski C, Wang J, Leetmaa A, Reynolds R, Jenne R, Joseph D. 1996. The NMC/NCAR 40-year reanalysis project. *Bulletin of the American Meteorological Society* **77**:437-471.
4. Kistler R, Kalnay E, Collins W, Saha S, White G, Woollen J, Chelliah M, Ebisuzaki W, Kanamitsu M, Kousky V, Van Den Dool H, Jenne R, Fiorino M. 2001. The NCEP-NCAR 50-year reanalysis: Monthly means CD-ROM and documentation. *Bulletin of the American Meteorological Society* **82**:247-268.
5. Kutiel H, Benaroch Y. 2002. North Sea Caspian Pattern (NCP) - an upper level atmospheric teleconnection affecting the eastern Mediterranean: Identification and definition. *Theoretical and Applied Climatology* **71**:17-28
6. Kutiel H, Maheras P, Türkeş M, Paz S. 2002. North Sea Caspian Pattern (NCP) - an upper level atmospheric teleconnection affecting the eastern Mediterranean: Implications on the regional climate. *Theoretical and Applied Climatology* **72**:173-192
7. Kutiel H, Türkeş M. 2005. New evidence for the role of the North Sea − Caspian Pattern on the temperature and precipitation regimes in continental central Turkey. *Geografiska Annaler. Series A: Physical Geography* **87**: 501-513.
8. Rosenblum MG, Pikovsky AS, Kurths J. 1996. Phase synchronization of chaotic oscillators. *Physical Review Letters* **76**:1804-1807.
9. Rybski D, Havlin S, Bunde A. 2003. Phase synchronization in temperature and precipitation records. *Physica A* **320**:601-610.
10. Tatli H, Dalfes HN, Mentes SS. 2005. Surface air temperature variability over Turkey and its connection to large-scale upper air circulation via multivariate techniques. *International Journal of Climatology* **25**:331-350.
11. Wallace JM, Gutzler DS. 1981. Teleconnections in the geopotential height field during the Northern Hemisphere winter. *Monthly Weather Review* **109**:784-812.
12. Wanner H, Bronnimann S, Casty C. 2001. North Atlantic Oscillation - concepts and studies. *Surveys in Geophysics* **22**:321-382.

VARIATIONS OF HEAVY RAINFALL AND SEA SURFACE TEMPERATURE IN THE KOREAN COAST UNDER THE PASSING OF TYPHOON WITH STRONG WIND

Hyo Choi

Kangnung National University Kangnung, Korea, choihyo@kangnung.ac.kr

ABSTRACT

As typhoon passes through Korean peninsula or its vicinity more than ten times per year, severe disasters in summer, especially June through September occur due to heavy precipitation in land and variation of sea water quality and sea surface temperature (SST) in the coastal sea. Numerical prediction on rainfall event under the influence of typhoon number 18-Sonda with a pressure of 935hPa, with a maximum speed of 46m/s, which passed from Guam island in the South China Sea through the coastal cities adjacent to the East Sea of Korea from September 5 through 8, 2004 was carried out using a three-dimensional non-hydrostatic numerical model, MM5-version 3.7. As the center of the typhoon approached Kyusu island of Japan, precipitation amount in the coastal cites near the southeastern part of Korean peninsula from September 6 until 1400LST, September 7 primary increases by heavy clouds formed by the typhoon, through directly the supply of moisture induced by synoptic-scale easterly wind under a cyclonic circulation.

Secondary, it was due to much cooling and condensation of moist air induced by upslope wind from the East Sea toward the top of the mountains in the west, resulting in heavy precipitation in the whole coastal region and sea. Under the influence of the typhoon, strong wind band occurs in the upper quadrant of right hand side in the frontal area of typhoon on a typhoon track. This strong marine surface wind can cause more moisture advection from the sea surface into the inland. Under this circumstance, surface wind induced by cyclonic circulation becomes windstorm greater than 10m/s in the coastal region for several hours.

The model result was compared with monitoring data and radar echo at dense monitoring sites established by Korean Meteorological Administration. Under the influence of heavy precipitation in the coastal sea, SST distributions using GOES satellite pictures have also been changed before and after the passage of the typhoon through Korean Strait. Daily mean of SST in the eastern coastal sea has 1^0C difference between before and after the passage of the typhoon near the coastal sea. The distribution of 7 days SST anomaly is much changed. When typhoon passes near Korean peninsula, precipitation amount in general reaches more than 100mm per 3 hours, resulting in occurrence of flood in the mountains, urban area and even coastal region. Driving mechanism of heavy rainfall and forecasting of typhoon track will be further discussed in detail.

EVALUATIONS ON AIR POLLUTION FROM SHIPS FOR GLOBAL AND BOSPHORUS: EFFECTS ON CLIMATE CHANGE

Hüseyin TOROS and Ali DENİZ

Department of Meteorology, Faculty of Aeronautics and Astronautics, Istanbul Technical University, 34469, Maslak, Istanbul, Turkey.
toros@itu.edu.tr; denizali@itu.edu.tr

ABSTRACT
One of the important environmental problems is air pollution from sea transportations, because of the transportation of goods has recently been increasing by ships. Usually, ships' emission is harmful for human health and animals, plants and the others. The air pollution in the all over the world, emissions of nitrogen oxides (NO_x), sulphur oxides (SO_x), carbon dioxide (CO_2), volatile organic compound (VOC) from shipping due to combustion of marine fuels are effective for air pollution. The ships that burn tons of fuel per hour, generating large volumes of pollution, global warming gases and black carbon, contribute to climate change. According to the International Maritime Organization (IMO) radioactive forcing due to CO_2 emissions from ships indicates that ships may account for 1.8 per cent of the global. European flagged ships emitted almost 200 million tones of CO_2, 2.6 million tons of SO_2 and 3.6 million tons of NO_x in 2000.

In this study the role of Bosphorus is emphasized for sea pollution from ships, which are more than 50000 are passing from the Bosphorus and more than percentage %10 of them are tanks.

Keywords: Sea Transportation, Air Pollution, Climate Change.

INTRODUCTION

Since the beginning of the industrialization population and sea transportation have been increasing and they cause for air pollution, which is some frightened for ecological future because of climate change. Therefore climate change is one of the most difficult environmental problems faced by humankind. There are a lot of scenario types about air pollution in the world; they are quality, quantity, transportation, possible effects and the others. The issue of controlling air pollution form ships was discussed in the International Convention for the Prevention of Marine Pollution (MARPOL) in the 1973. However, it was decided not to include regulations concerning air pollution at the time. Long and short distance shipping plays important roles in facilitating international trade transportation over the world. Cargo transport by ships is about 70 percent of all trade between the European Union (EU) and the rest of the world. More than 30,000 ships with tonnage at or above 250 gross registered tons operate in European waters in a given year. Air pollution like ozone and fine aerosol particles, produced as secondary products of shipping emissions, can be transported long distances in the atmosphere, from sea to land, and even from one continent to another, (Harrison et al., 2004; Derwent et al., 2004; Jaffe et al., 2003; ENTEC 2002; Qinbin et al., 2002; Davies et al. 2000).

Environmental and Engineering Consultancy (ENTEC) has been studied about ship emissions of SO_2, NO_x, CO_2 and hydrocarbons in the North Sea, Irish Sea, English Channel, Baltic Sea, Black Sea and Mediterranean, as well as quantifying in port emissions of these pollutants plus particulate matter; to determine these emissions for all vessels as well as separately for each vessel type and flag state. This should separately consider, all vessel movements, where the starting port and destination port are both in the Community, where the starting port is inside the Community but the destination port is not, where the destination port is in the Community but the starting port is not and where no stops at any Community port are undertaken; Estimation of the effects of the International Convention for the Prevention of Marine Pollution (MARPOL) from ships agreement and additional future scenarios upon emissions, principally sulphur dioxide and particles, in the North Sea and Baltic Sea and other European seas, to present these emissions in tabular and map form; to undertake a market survey of low sulphur marine distillates, and to investigate the feasibility of ships storing and using multiple grades of marine distillates, (ENTEC, 2002; Acid News, 2006).

Emissions from international shipping in European waters show a steady increase. Since 1990, ship emissions of SO_2 have gone up from 1.8 to 2.6 million tonnes, and those of NO_x from 2.6 to 3.7 million tones – in both cases an increase of more than 40 per cent, (Acid News, 2006). Ships are fast becoming the biggest source of air pollution in the EU. According to the Commission of the European Communities (CEC) unless more action is taken they are set to emit more than all land sources combined by 2020, (CEC, 2005).

As the International Maritime Organization (IMO) notes in their study of greenhouse emissions from ships, there is an increasing awareness of the impacts of shipping emissions on onshore air quality. An estimated 85 percent of international shipping traffic occurs in the northern hemisphere, and 70 percent of that is within 400 km of land. Much of the shipping activity and associated emissions occur near major urban areas, many of which are already struggling with air quality problems (IMO, 2000). In 2000 EU flagged ships also emitted almost 200 million tonnes of carbon dioxide. This is significantly more than emissions from EU aviation. Ships all over the world burns million tons of fuel per year, generating large volumes of global warming gases likes CO_2 that contribute to climate change, (ENTEC, 2005).

The ships passing from the Bosphorus (İstanbul and Çanakkale) contribute sea, air, noise pollution and other environmental risks like maritime accidents. Recently the number of ships passing from İstanbul and Çanakkale increases and these shipping activities contribute significantly to the air pollution in the Bosphorus. Emissions of nitrogen oxides (NO_x), sulphur oxides (SO_x) from shipping due to combustion of marine fuels contribute to air pollution in the form of SO_x and NO_x and particulate matter, harming the environment through acidification as well as human health, animal and plant life particularly around coastal areas. More than 50000 ships are passing from the Bosphorus and more than percentage %10 of them are tanks. In this study numbers of ships by ships are given and the results may help environmental scientists and policy makers, (Toros, 2000; Toros et al., 2006; Güven and Özturk, 2005).

STUDY AREA AND DATA

Scientist engaged in finding the affects of air pollution in sea transportation, estimate and design a model and to estimate its environmental effects. Engineers, on the other hand, are interested in finding cheaper but least harmful systems. Emission of air pollution from shipping due to combustion of marine fuels contribute to air pollution in the form of NO_x, SO_x, PM, CO_2, and VOC cause negative effect on climate change. SO_x and NO_x and particulate matter.

The Turkish Straits are one of the most crowded sea lanes in the world used for international navigation. The Bosphorus Strait is a geological strait separating the European and the Asian parts of Istanbul and it lies between the Black Sea and the Sea of Marmara, (Fig. 1). Ships which pass through the Bosphorus and ships going to European sea and all parts of the world pollute atmosphere in ways which should not be underestimated.
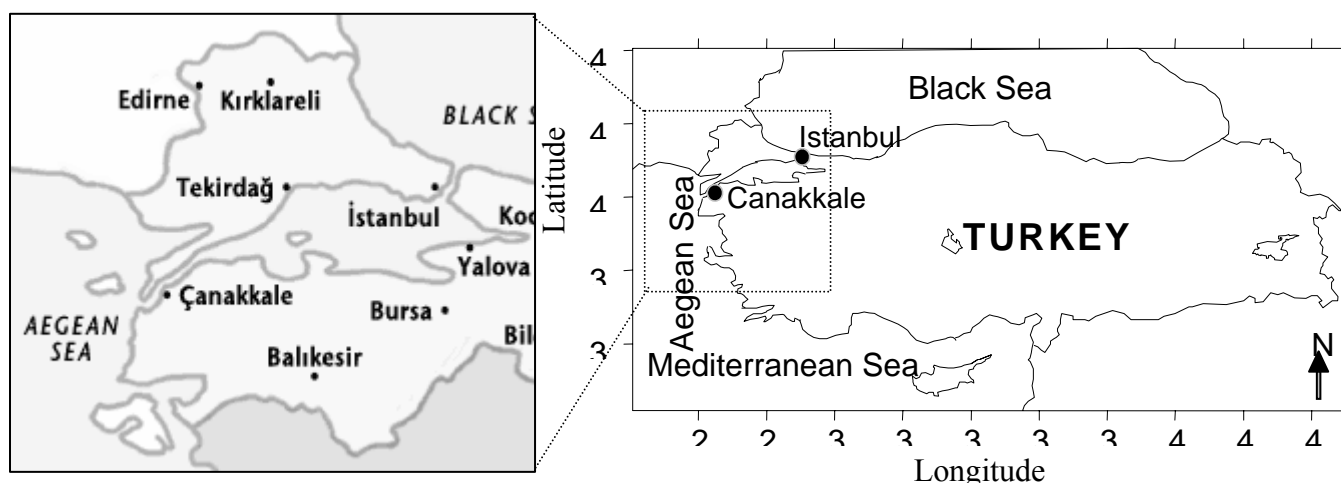
Figure 1. The location of Turkish Straits.

The Turkish Straits, comprising the Strait of Çanakkale and the Strait of Istanbul through the Black, Marmara, Aegean and Mediterranean Sea, are unique in many respects in the world. The Turkish Straits are one of the most crowded, hazardous, potentially dangerous and difficult waterways in the world for marines. All the dangers and obstacles characteristic of narrow waterways are present and acute in this critical sea lane. The Strait of Istanbul is approximately 31 kilometers long average depth 35 meters average width 1.5 km at the narrowest point is about 700 meters. The length of the strait of the Çanakkale is about 70 kilometers with a general width ranging 1-2 kilometers, (DM, 2004; TMPA, 2006; Akten, 2003; Özçayır, 2001; Yönsel, 2001).

With in ten years on the average annually 50000 ships (10 per cent being tankers) passed through the Bosphorus. The total figures of ships passing through from the strait of Istanbul and Çanakkale was shown in Table 1 and 2.

Table 1. Total Figures for the Strait of Istanbul 1995-2003, (TMPA, 2006).

YEARS	TOTAL	Took Pilot	SP report	Over 200m.	Over 500 GT	Direct Passed	Tankers
1995	35459	8292	12382	8164	31662	23249	N/A
1996	36198	10307	13473	8304	34789	24061	5658
1997	36198	10307	13473	8304	34789	24061	5658
1998	38777	11448	17692	2394	37295	25136	6546*
1999	40582	10002	24533	2568	44354	26900	5445
2000	41561	11130	33861	2697	40163	27033	5543
2001	39249	10703		2960		26452	7079
2002	42669	12164	42477	3665	41980	29900	7637
2003	42648	13020	42648	38925	42530	29117	8114

*This value includes all vessels carrying dangerous cargo

Table 2. Total Figures of Passages for the Strait of Çanakkale 1995-2003, (TMPA, 2006).

YEAR	Total	Used Pilot	SP report	Longer than 200m.	Over 500 GT	Direct Passed	Tankers
1995	46954	17772	9571	6491	40724	24325	-
1996	49952	20317	12777	7236	44636	23755	4248
1997	50942	19752	15503	6487	45849	24568	4303
1998	49304	18881	24432	1943	44829	24561	5142*
1999	47906	18424	30619	2168	44354	26323	4452
2000	48079	19209	38574	2203	44734	26858	4937
2001	42637	17767		2453		26113	6516
2002	47283	19905	44728	3113	45350	29398	7427
2003	46939	21175	45340	2923	45157	28961	6578

*Includes vessels carrying dangerous cargo.

Air pollution from ships depends on the vessel, vessel type, engine type, vessel size, and the quality of fuel oil and sea species for example the Bosphorus like a river. For example the ship going from Mediterranean to Black sea must use more fuel oil to burn and that means more air pollution. Also the effects of air pollution from ships depend on meteorological parameters in the region. Truck versus ship emissions average vehicle and fuel, a ship will let out 30-50 times more sulphur per ton-kilometers than a truck. When diesel becomes even cleaner in 2005, the difference will increase to 150-300 times. Turning to nitrogen oxides, ships now release about twice as much per ton-kilometer as the latest truck models, and the difference is set to increase, (Table 3). In 2005, the emission standards for trucks in the EU will be cut from the present 5.0 g/kWh to 3.5, and in 2008 to 2.0 g/kWh, (NTM, 2006).

Table 3. Emissions from trucks on long hauls with different EU standards for emissions and from cargo vessels of various sizes. Figures in grams per ton-kilometer, (NTM, 2006).

	CO_2	PM	SO_2	NO_x	VOC
Heavy truck with trailer:					
Before 1990	50	0.058	0.0093	1.00	0.120
Euro 0 (1990)	50	0.019	0.0093	0.85	0.040
Euro 1 (1993)	50	0.010	0.0093	0.52	0.035
Euro 2 (1996)	50	0.007	0.0093	0.44	0.025
Euro 3 (2000)	50	0.005	0.0093	0.31	0.025
Cargo vessel:					
large (>8000 dwt)	15	0.02	0.26	0.43	0.017
medium (2000-8000 dwt)	21	0.02	0.36	0.54	0.015
small (<2000 dwt)	30	0.02	0.51	0.72	0.016
RoRo (2-30 dwt)	24	0.03	0.42	0.66	0.029

Emissions are average in each case. Trucks: maximum overall weight 40 tons, loading 70 per cent, operating on diesel with a sulphur content of 300 ppm. Cargo vessel: bunker oil with and average sulphur content of 2.6 per cent, no cleaning of NO_x, (NTM, 2006).

Table 4 shows the growth of emissions of air pollutants (NO_x, SO_2, CO_2, HC, PM) and low and high estimation values of next future. Annual growth in shipping movements for future years, which estimated between 1.5% and 3% growth per annum in vessel movements for the period 2000 – 2010. The estimations of NO_x, SO_2, CO_2, HC and PM are 4.649, 3.294, 200.105, 171 and 28 million tons respectively, (ENTEC, 2002).

Table 4. Past and future estimated shipping emissions scenario in 1990, 2000 and 2010, (ENTEC, 2002).

	NO_x	SO_2	CO_2	HC	PM (in port)
1990	2,808	2,001	122,115	104	16
2000	3,617	2,578	157,298	134	21
2010-Low	4,015	2,845	172,791	147	24
2010-High	4,649	3,294	200,105	171	28

EVALUATION OF RESULTS

When the air pollution emitted from ships began to threaten the ecosystem, so scientist started to study the dimension of its effects and low maker, on the other hand, tried to enact lows which would minimize its effects, because of the quantity of emission from ships depends on the type of the ship, the quality of fuel oil and the largeness of the load carried. Sea transportation is preferred for carrying oil, oil products and the largeness and heavy load. Due to SO_2 and NO_x emissions are responsible for acid deposition, which can be harmful to the environment, as well as particulate matter harmful to health. NOx and VOC emissions

contribute to the formation of ground-level ozone harmful to health and to the environment. NO_x emissions contribute to environmentally damaging eutrophication. CO_2 emissions contribute to global climate change. Halon emissions damage the ozone layer.

The air pollution emissions of ships passing through the Turkish Straits, strategically situated between Asia and Europe, not only have harmful effects on the people but cause a great deal of damage to historical objects.

The purpose of this studying the air pollution emission from ships is to enlighten the people of its harmful effects and to encourage them to use less harmful fuel especially in transportation liquid or gaseous matters through the pipe system.

People's health, ecology, destruction of historical objects, and other problems like climatic change created by air pollution is a threat of the world's future. Unless we take steps to obliterate it we will have to face the consequences. As a result for our future we must do sets out a number of actions to reduce the air pollution from shipping to acidification, ground-level ozone, eutrophication, health, ozone depletion and climate change.

REFERENCES

Acid News, 2006. The Swedish Society for Nature Conservation, No. 3, October,Göteburg, Sweden.

Akten, N., 2003. The Strait of İstanbul (Bosphorus): The seaway separating the continents with its dense shipping traffic", Turkish Journal of Marine Sciences", Published by Institute of Marine Sciences and Management, University of İstanbul, Volume 9 (3): 250, 263 (2003).

CEC, 2005. The Communication on Thematic Strategy on Air Pollution and The Directive on "Ambient Air Quality and Cleaner Air for Europe", Commission Staff Working Paper, Ship emissions assignment report, p160.

Davies, M.E., Plant, G., Cosslet, C., Harrop, O. and Petts, J.W., 2000. Study on the economic, legal, Environmental and practical implications of a European Union system to reduce ship emissions of SO2 and NOx. Final report for European Commission Contract B4-3040/98/000839/MAR/B1, 2000.

Derwent, R.G., Stevenson, D.S., Collins, W.J., Johnson, C.E.(2004), "Intercontinental transport and the origins of the ozone observed at surface sites in Europe," Atmos. Environ 38:1891.

DM, 2004. T.C. Başbakanlık, Denizcilik Müsteşarlığı, Seyir Güvenliği Daire Başkanlığı, Ankara, (www.cankaya.gov.tr), 2004.

ENTEC, 2002. Quantification of emissions from ships associated with ship movements between ports in the European Community. Study for the European Commission. (www.europa.eu.int/comm/environment/air/background.htm#transport)

ENTEC, 2005. European Commission Directorate General Environment Service Contract on Ship Emissions: Assignment,Abatement and Market-based Instruments Contract No: 070501/2004/383959/MAR/C1 Task 1 - Preliminary Assignment of Ship Emissions to European Countries Final Report August 2005, Entec UK Limited.

Guven, K.C. and Ozturk, B. , 2005: Cleaning Oil Pollution from Sea, in: Sea Pollution, Turkish Marine Research Foundation Publications, Istanbul, No: 21, 147-204.

Harrison, D., Radov, D. and Patchett, j., 2004. Evaluation of the Feasibility of Alternative Market-Based Mechanisms To Promote Low-Emission Shipping In European Union Sea

Areas. National Economic Research Associates, NERA Economic. Final Report March 2004

IMO, 2000. MARNEK Det Norske Veritas, Econ Centre for Economic Analysis, and Carnegie Mellon University for International Maritime Organization (IMO), Marine Environment Protection Committee (MEPC) 45(8) Agenda Item #2. Study of Greenhouse Gas Emissions from Ships.

Jaffe, Dan, I. McKendry, T. Anderson, H. Price (2003), "Six 'new' episodes of trans-Pacific transport of air pollutants," Atmospheric Environment 37:391–404.

NTM, 2006. http://www.ntm.a.se/english/eng-index.asp.

Özçayır, Z.O. (2001, January). What are the dimensions of pollution at Black Sea. Turkish Shipping World, 59-61

Qinbin Li, D. Jacob, I. Bey, P. Palmer, B. Duncan, B. Field, R. Martin, A. Fiore, R. Yantosca, D. Parrish, P. Simmonds, and S. Oltmans (2002), "Transatlantic transport of pollution and its effects on surface ozone in Europe and North America," Journal of Geophysical Research Vol. 107, "NO. D13, 10.1029/2001JD001422.

Ship Emissions Assignment Report, P. 160, 2005.

TMPA, 2006. Turkish Maritime Pilots' Association Home Page. http://www.turkishpilots.org.tr/ingilizcedernek/DOCUMENTS/statistics.htm

Toros, H., "İstanbul'da Asit Yağışları, Kaynakları ve Etkileri", Doktora Tezi, 110s., İTÜ, 2000.

Toros, H., Deniz, A., Kadıoğlu, M., Akhisar, İ., 2006. Deniz Ulaşımının Hava Kirliliği Üzerine Etkisi. VI. Ulusal Temiz Enerji Sempozyumu, 25-27 Mayıs 2006. Isparta.

Yönsel, F. (2001, November). Priority issue of the day:Pollution.. Turkish Shipping World, 94-97